

Evidence for a Two-Dimensional Quantum Glass State at High Temperatures

Google Quantum AI and collaborators
(Dated: March 17, 2026)

Disorder in quantum many-body systems can drive transitions between ergodic and non-ergodic phases, yet the nature—and even the existence—of these transitions remains intensely debated [1–11]. Using a two-dimensional array of superconducting qubits, we study an interacting spin model at finite temperature in a disordered landscape, tracking dynamics both in real space and in Hilbert space. Over a broad disorder range, we observe an intermediate non-ergodic regime with glass-like characteristics: physical observables become broadly distributed and some, but not all, degrees of freedom are effectively frozen. The Hilbert-space return probability shows slow power-law decay, consistent with finite-temperature quantum glassiness. In the same regime, we detect the onset of a finite Edwards-Anderson order parameter and the disappearance of spin diffusion. By contrast, at lower disorder, spin transport persists with a nonzero diffusion coefficient. We furthermore track wavefunction statistics across the critical point, showing an evolution from the Porter-Thomas distribution in the ergodic phase to power-law scaling in the glassy phase. Our results show that there is a transition out of the ergodic phase in two-dimensional systems that does not coincide with the localization transition.

Glassy behaviour emerges when a system fails to equilibrate on experimentally relevant timescales, leading to slow relaxation and frozen degrees of freedom [12–14]. Typically this behaviour is due to competing interactions (frustration). Qualitatively, the phase space of classical glasses is separated into an exponentially large number of compartments, \mathcal{N} , that trap the system. The configurational entropy is extensive, $S_{\text{conf}} = \ln(\mathcal{N}) \propto n$, where n is the number of atoms. Despite phase space compartmentalization, classical glasses display aging and rejuvenation phenomena [15, 16]. This implies the existence of rich dynamics within each compartment. For example, tunnelling between configurations with nearby energies (also known as ‘two-level systems’) generates low frequency $1/f$ noise [17–19]. Like their classical analogue, quantum glasses also exhibit hallmark features such as history dependence, broadly-distributed local observables, and slow, power-law relaxation. Quantum glasses are characterized by Hilbert space fragmentation, where some degrees of freedom remain frozen while others fluctuate, giving rise to rich non-ergodic dynamics [20]. The exponentially-growing volume of Hilbert space with system size, however, complicates the study of these systems. Quantum simulation, as applied in this work, offers a unique opportunity to correlate the real space properties of quantum glasses with the properties of the wavefunctions in Hilbert space.

The breakdown of ergodicity is a hallmark feature of glasses. The transition to non-ergodicity in quantum systems has historically been studied in the context of many-body localization (MBL), in which all wavefunctions become completely localized. Numerical and theoretical approaches to studying this transition are well-established [21–26], yet definitive conclusions remain elusive. The original approach [1] focused on frozen transport at low temperatures ($T > 0$), whereas most subsequent studies have examined a simplified scenario in the infinite-temperature limit ($T \rightarrow \infty$). In the absence of a controlled analytical theory for realistic systems, one

must rely on numerical simulations, which often yield conflicting results regarding the location—or even the existence—of a transition from an ergodic state to an MBL state with frozen dynamics. Between these extremes, an *intermediate* class of eigenstates, referred to here as Non-Ergodic Extended (NEE), has been proposed (Fig. 1). The NEE wavefunction has an exponentially large support that is nonetheless parametrically smaller than the full Hilbert space dimension. These distinctive Hilbert space features directly manifest in the transport properties of the system, further distinguishing the NEE phase from the fully localized MBL state. The high Hilbert space connectivity—while insufficient for macroscopic particle transport—provides the necessary channels for energy transport and dephasing, features that are entirely obstructed in a fully localized MBL state. The NEE state can also be contrasted with an ergodic state, which explores all of Hilbert space. While the field is actively debating the fate of NEE states in the infinite-time and thermodynamic limit (see, e.g., Ref. [27]), their robust presence in theoretical studies across a wide range of models, system sizes, and timescales invites a finite-size experimental study. Such a pursuit might reveal phenomena that fall outside the traditional binary of ergodic and localized phases.

NEE states sharing support over the same Hilbert space volume form a ‘cluster’. Because the volume of these clusters is exponentially large in system size, there are many eigenstates within each cluster, and as a result they exhibit a significant overlap driving fast entanglement growth. Distinct clusters, however, are weakly overlapping, and as such the number of states entangled in this process remains restricted to a small fraction of the total Hilbert space. The number of clusters \mathcal{N} at the same energy is exponentially large, with entropy $S = \ln(\mathcal{N}) \propto n$; this matches the configurational entropy of a glass. By examining the properties of a two-dimensional ($2D$) disordered spin system at high temperature, we show that the commonalities between

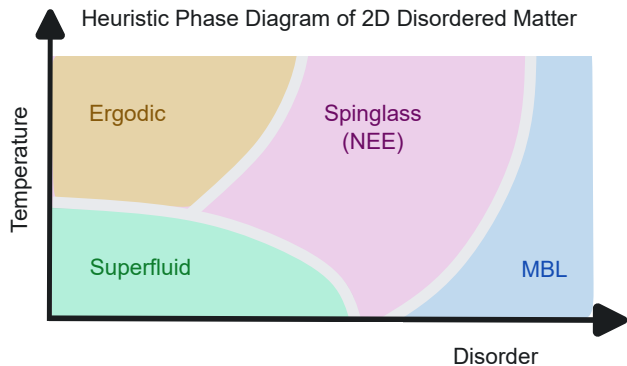


FIG. 1: Phase Diagram. At low temperatures and weak disorder, the system exhibits long-range order, while strong disorder localizes the bosons. At high temperatures, weak disorder yields an ergodic diffusive phase; increasing disorder drives a transition to a glassy non-ergodic state with finite Edwards-Anderson order parameter, and ultimately to a fully frozen MBL phase.

quantum glasses and NEE states extend beyond a shared configurational entropy. In fact, our data suggest that what the classical literature calls a ‘quantum glass’ and what many-body physicists call a ‘non-ergodic extended state’ might in fact be two perspectives on the same physical state. We support this conclusion with both real space measurements (magnetization, diffusivity) and Hilbert space diagnostics (return probability, wavefunction statistics).

NEE plausibility. Crucial for the understanding of classical glasses is the theoretical solution of infinite-range models, which reproduce the extensive configurational entropy of classical glasses below the transition [14]. Similarly, the existence of NEE states has been convincingly demonstrated in various random matrix models and infinite range systems [28–35]. A key feature of these theoretical models is that the Hamiltonian is a full matrix spanning the entire Hilbert space, with the number of independent random parameters scaling as $\sim N$, where N is the Hilbert-space dimension. In contrast, quantum spin chains and arrays exhibit extreme sparsity in their Hilbert-space Hamiltonians, scaling as $\sim \ln(N)$. This sparsity introduces strong correlations between matrix elements, complicating direct application of conventional random matrix frameworks to realistic glasses in 1, 2 or 3 dimensions. In this respect the situation is very similar to the classical theory of (spin) glasses, in which reliable theory is limited to infinite range models [36], which nonetheless provide some qualitative understanding of real systems.

Early indications of non-ergodic phases in numerical studies appeared as sub-diffusive transport in one-dimensional (1D) models [37–39], as well as in Josephson junction chains [40, 41]. Qualitatively similar features were discussed in Ref. [42] in terms of a pre-thermal regime. More recently, theoretical arguments support-

ing NEE states in random spin chains have been presented in the literature [43, 44]. Whether non-ergodic states exist in many-body systems in more than one spatial dimension ($D > 1$) remains an open and debated question. Several works have argued against the stability of MBL phases in higher dimensions [24, 45–47]. However, these arguments do not rule out a breakdown of ergodicity, as the absence of an MBL phase does not preclude NEE behaviour. Generally, numerical simulations of quantum glasses in the NEE state are very difficult because of the exponential volume of the relevant Hilbert space involved.

Recent advances in controllable quantum processors [48] have enabled numerous studies of ergodicity and its breakdown. Most MBL investigations have focused on the real-space phenomenology, particularly by studying the relaxation rates and asymptotic behaviour of population imbalance [49–53]. These experiments are demanding in terms of the number of disorder realizations and repetitions required, readily adding up to $\sim 10^{10} - 10^{12}$ shots. Superconducting qubit arrays make it possible to directly probe complex dynamics in Hilbert space with fast data rates of tens of kHz [54]. In this work, by studying the dynamics both in Hilbert space and in the real (2D) domain, we find evidence for the existence of an NEE state in spin dynamics with strong disorder at $T = \infty$.

The dynamics of excitations in a 2D nearest-neighbour qubit array can be modeled by the spin Hamiltonian

$$H = -J \sum_{\langle i,j \rangle} (S_i^+ S_j^- + S_i^- S_j^+) + \sum_i h_i S_i^z, \quad (1)$$

where S_i^α are spin- $\frac{1}{2}$ operators, h_i are site-dependent random disorder drawn from a box distribution of width W and zero mean, and J denotes the nearest-neighbour coupling strength on the square spin lattice. The XY coupling, which favours long-range XY order, competes directly with the applied field in the Z direction. Building on prior studies and general physical considerations, a phase diagram of this interacting spin model can be proposed, as shown in Fig. 1. At low temperature and zero disorder, the kinetic term drives the system into a long-range ordered phase corresponding to a superfluid of hard-core bosons. Large-scale quantum Monte Carlo simulations at $T = 0$ [55] confirm that superfluidity persists even in the presence of weak disorder, $w \equiv W/J \leq 19$. At very strong disorder, the bosons are possibly localized; the existence of an MBL phase or lack thereof is not within the scope of this paper. For intermediate values of disorder, we propose the existence of a phase characterized by glassy, non-ergodic extended states with a nonzero Edwards-Anderson order parameter.

Glassy behaviour in magnetization. We begin our experimental studies by measuring the local magnetization in real space, a quantity that is readily accessible on most quantum processors. Starting from a 59-qubit product

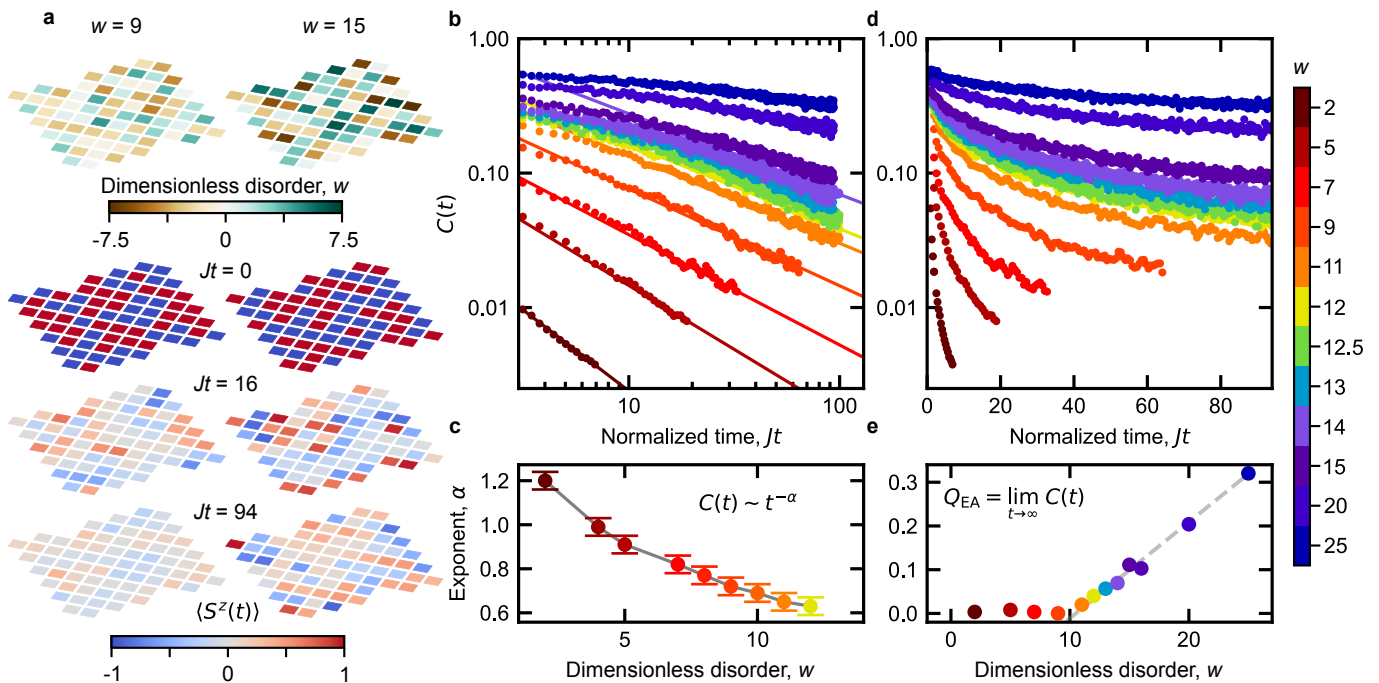


FIG. 2: Evidence of glass formation in the frozen magnetization. **a**, Temporal evolution of magnetization for disorders of $w = 9$ and $w = 15$ (corresponding disorder patterns showed on top), revealing slower relaxation at the higher disorder. **b**, Time dependence of the spin glass correlation function $C(t)$, showing power law relaxation of $C(t)$ in the ergodic phase. **c**, Disorder-dependence of the dynamic exponent α that describes the power-law decay of $C(t)$. **d**, Same as **b**, but with linear axis, revealing the absence of complete relaxation at higher disorders. **e**, The Edwards-Anderson order parameter, $Q_{\text{EA}} = C(\infty)$, as a function of w shows an abrupt change in slope near $w = w_c \simeq 10$. Q_{EA} is extracted from fitting $C(t)$ with a decaying functional form (exponential with or without a power-law prefactor, see SI) with a constant offset.

state at $t = 0$, we consider the relaxation of the spin distributions, shown in Fig. 2a for two different disorder strengths, $w = 9$ and $w = 15$. The subsequent spatial maps show that the magnetization profile relaxes almost completely in the case of low disorder ($w = 9$), whereas substantial magnetization remains frozen at higher disorder ($w = 15$). This is a first indication of reduced ergodicity. To further study this contrasting behaviour, we next plot the dynamic spin-glass correlation function,

$$C(t) = \overline{\langle S_i^z(0) S_i^z(t) \rangle^2}, \quad (2)$$

for a wide range of disorder values (Fig. 2b). In the weakly disordered regime, the correlation function is found to obey a power-law decay, with an exponent α that decreases from unity to about $2/3$ as w approaches a critical value, $w_c \sim 10$ (Fig. 2c). For values above w_c , however, the decay deviates from power-law behaviour (see further analysis in SI) and saturates at a non-zero value of the Edwards-Anderson order parameter, $Q_{\text{EA}} = C(t \rightarrow \infty)$, as is more clearly observed with a linear time axis (Fig. 2d). This behaviour is quantified in Fig. 2e, where we show the extracted Q_{EA} : while Q_{EA} is found to be very small in the ergodic regime, we observe a clear change to linear growth with disorder for $w \gtrsim w_c$, consistent with a transition or sharp cross-over.

The observed freezing-in of magnetization dynamics is in qualitative agreement with earlier observations [50].

Return probability. While real-space magnetization dynamics have provided valuable information about disorder-induced slowdown in previous studies [52, 53], and enabled us to characterize the w -dependence of Q_{EA} , our ability to fully characterize the disordered regime from this perspective is limited. Moreover, drawing definite conclusions has previously been made challenging by small values of the decay exponents ($10^{-2} - 10^{-1}$), and thus modest variation over available experimental timescales [52, 53]. To gain a more comprehensive picture, we move beyond these real-space metrics to probe the system's dynamics in Hilbert space by measuring the return probability,

$$R(t) = |\langle \Psi(t) | \Psi(0) \rangle|^2, \quad (3)$$

which quantifies ergodic behaviour in Hilbert space: in an ergodic system, the probability of returning to the initial state should quickly drop to the inverse number of states allowed by conservation laws. The measurement sequence proceeds as follows: (i) prepare an initial state in the form of a bit-string—an eigenstate of all S_i^z operators—corresponding to a total energy near the mid-

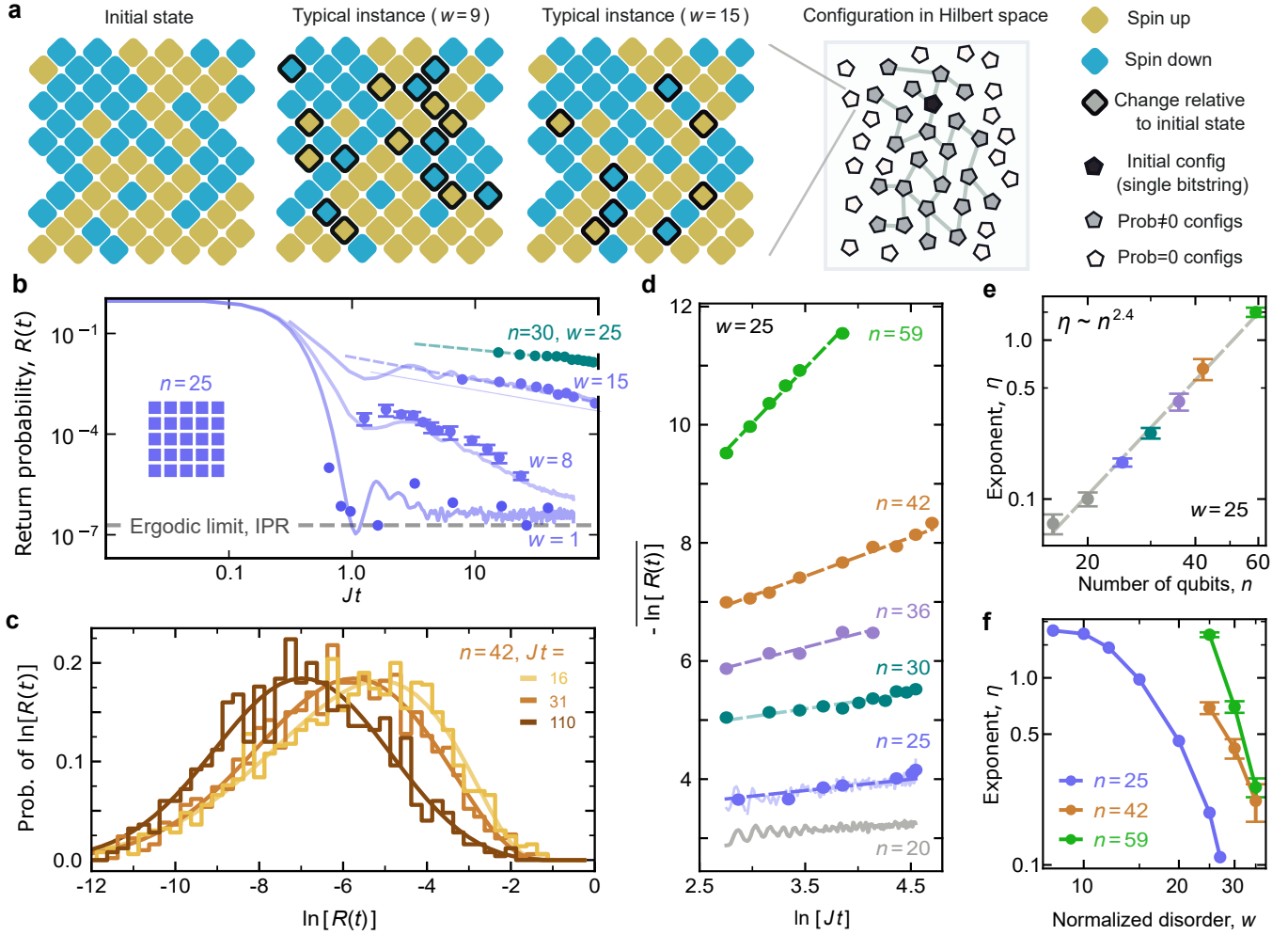


FIG. 3: Signatures of glassy behaviour in the return probability. **a**, Real-space measurement instances show that fewer spins are flipped when w is higher. The return probability is defined as the fraction of the measurements in which no spins are flipped. **b**, Time dependence of measured return probability for $n = 25$ (circles), which shows a local minimum (“correlation hole”) at low disorder, and power-law decay for larger w . Solid curves show results from exact numerical modeling, averaged over ~ 2500 disorder instances (100 for $w = 1$), while straight lines indicate power-law fits. **c**, Return probability on logarithmic scales shows a wide distribution, for $n = 42$ and at three different evolution times ($w = 30$). Solid lines are Gaussian fits. **d**, Time dependence of return probability $R(t)$ for a range of system sizes, displaying power-law dependence on time for $w = 25$. Solid straight lines show power-law fits. **e**, The power-law exponents extracted in **d** scale as $\eta \propto n^{2.4}$. **f**, Exponent η as a function of disorder for different system sizes. Continuous lines in panel **d**, $n = 20, 25$, as well as grey symbols in panel **e**, $n = 16, 20$ show results of numerical simulations; for $n = 25$ numerical results coincide with experimental ones.

dle of the energy spectrum; (ii) evolve the system under the Hamiltonian for time t ; (iii) measure in the same basis. Typical instances are shown for $w = 9$ and $w = 15$ in Fig. 3a: while many spins flip after a short amount of time for $w = 9$, only a few spins flip in the case of larger disorder. These pairs form effective two-level systems. To obtain the return probability $R(t)$, steps (i)–(iii) are repeated 10^5 – 10^6 times for a given $\Psi(0)$. The measured $R(t)$ depends on both the initial state $\Psi(0)$ and the realization of the random fields h_i . To determine its probability distribution, we averaged over many initial bit-strings

and randomized field configurations—typically $\sim 10^3$ realizations in the non-ergodic regime.

In the ergodic phase ($w = 1$), $R(t)$ is found to quickly decay to a very small value, which is the inverse of the total size of available Hilbert-space, i.e. $1/N = \binom{n}{n/2}^{-1} \sim 2^{-n}$. Before reaching that asymptotic value, $R(t)$ shows a shallow minimum around $Jt \sim 1$, consistent with a “correlation hole” [56, 57]. Note that resolving the small return probabilities in this regime ($w = 1$) requires a very large number of shots ($\sim 10^8$), making averaging over disorder very difficult. At larger disorders, $w > w_c \simeq 10$,

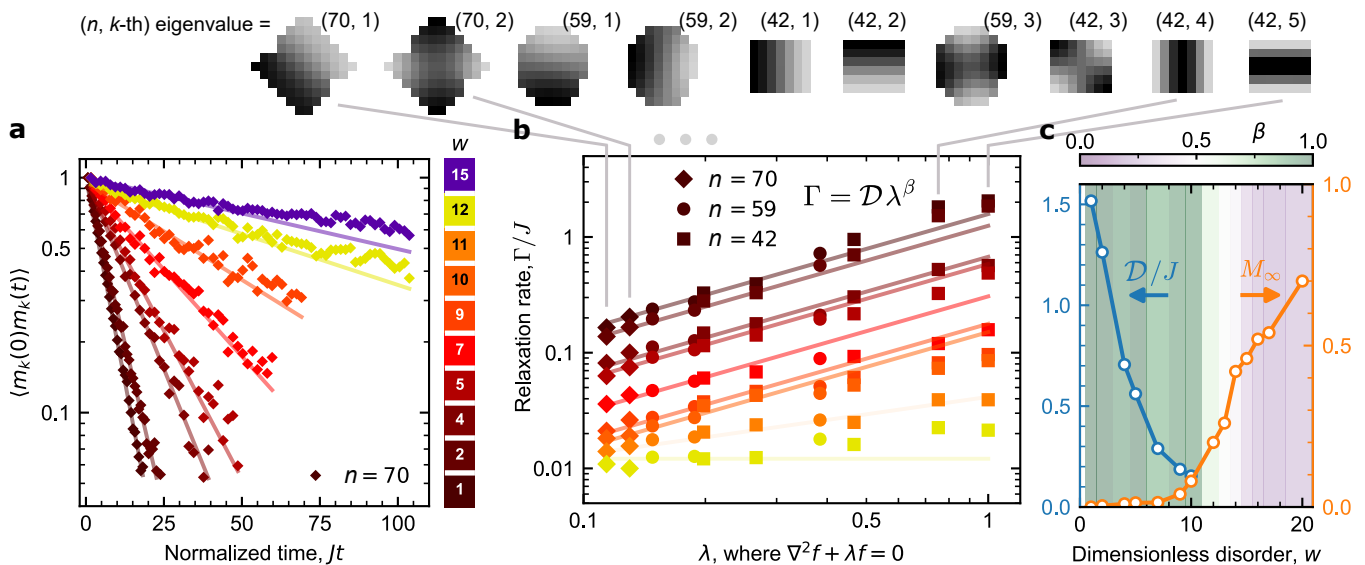


FIG. 4: Disappearance of diffusion at strong disorder. **a**, The measured relaxation of magnetization $\langle m_k(t)m_k(0) \rangle$ for the smallest eigenmode ($k = 1$) at several values of disorder ($n = 70$). **b**, Extracted relaxation rates for $n = 42, 59$ and 70 . Solid lines are fits using $\Gamma = \mathcal{D}\lambda^\beta$. **c**, The extracted diffusion constant \mathcal{D} (left axis) and non-zero frozen amplitude M_∞ (right axis). Background colours denote β , resulting from fitting data in **b** with $\Gamma = \mathcal{D}\lambda^\beta$. Diffusion applies for $\beta \approx 1$ and fails as β departs from unity and hence \mathcal{D} cannot be extracted above $w > 10$.

corresponding to non-ergodic phase, the correlation hole disappears and the return probability begins to hint at power-law dependence,

$$R_{\text{typ}}(t) \sim (Jt)^{-\eta} \quad (4)$$

Concomitantly, the return probability at any given time acquires a very wide distribution, even on the logarithmic scale (Fig. 3c). We fit the distribution of $\ln(R)$ with Gaussians to obtain the dependence of the typical $\ln \overline{R(t)}$ on system size, shown in Fig. 3d. We observe that the decay of the typical return probability is consistent with a power-law for all system sizes considered in the experiment. Importantly, the exponent η is found to grow superlinearly with n ,

$$\eta \approx \kappa(w) \cdot n^{2.4}, \quad (5)$$

as plotted in Fig. 3e for $w = 30$. At large w the exponent η decreases quickly (Fig. 3f), suggesting the appearance of a more localized phase at higher disorder strengths.

The observed power-law decay of R_{typ} at moderately strong disorder, $10 \leq w \leq 35$, is consistent with numerical results in 1D [58] and also in the ‘‘Quantum Sun’’ model [59, 60]. It differs qualitatively from both the oscillatory behaviour around a large value expected in the fully localized MBL phase, as well as the exponentially fast decay to very low values in the ergodic phase. This scaling is consistent with residual interactions between different spin pairs leading to dephasing and inelastic transitions (see Supplement). The power-law decay of

R_{typ} at long times suggests that the probability for a flip of any spin S_i^α grows logarithmically with time like $P_{\text{flip}} \sim (\eta/n) \ln(Jt)$; this behaviour generates spin noise with a $1/f$ power spectrum, known to be generic for glasses and spin glasses (see Supplement for supporting numerical simulations). Crucially, the noise power spectrum depends on the number of active spin pairs, resulting in a superlinear dependence of $\eta(n)$, as observed experimentally. Since non-interacting pairs would typically produce a linear scaling, this superlinearity supports the conclusion that the dephasing arises from internal dynamics rather than external noise.

Breakdown of diffusion. In the presence of locally conserved quantities, the relaxation of an ergodic state can be characterized by how each conserved quantity diffuses. Figure 4a shows the relaxation of the magnetization correlations, $\langle m_{k=1}(t)m_{k=1}(0) \rangle$, for various disorder strengths, after projecting (in post-processing) onto eigenmodes of the diffusion operator $-\nabla^2$ (the modes are indexed by k and take on eigenvalues λ ; owing to the irregular lattice geometry, they are computed numerically for each system size considered here, e.g., $\lambda_{\text{min}} = 0.114$ for $n = 70$). At weak disorder ($w = 1, 2, 4$), the magnetization decays exponentially $\propto e^{-\Gamma t}$. For moderate disorder ($w = 5, 7, 9$), the relaxation becomes slower, pointing to the onset of anomalous diffusion. At strong disorder, the decay is slower than exponential at long times, and the magnetization does not fully vanish; even at the longest time scales, a finite remanent amplitude M_∞ persists. An ‘‘effective’’ relaxation rate Γ can still be defined

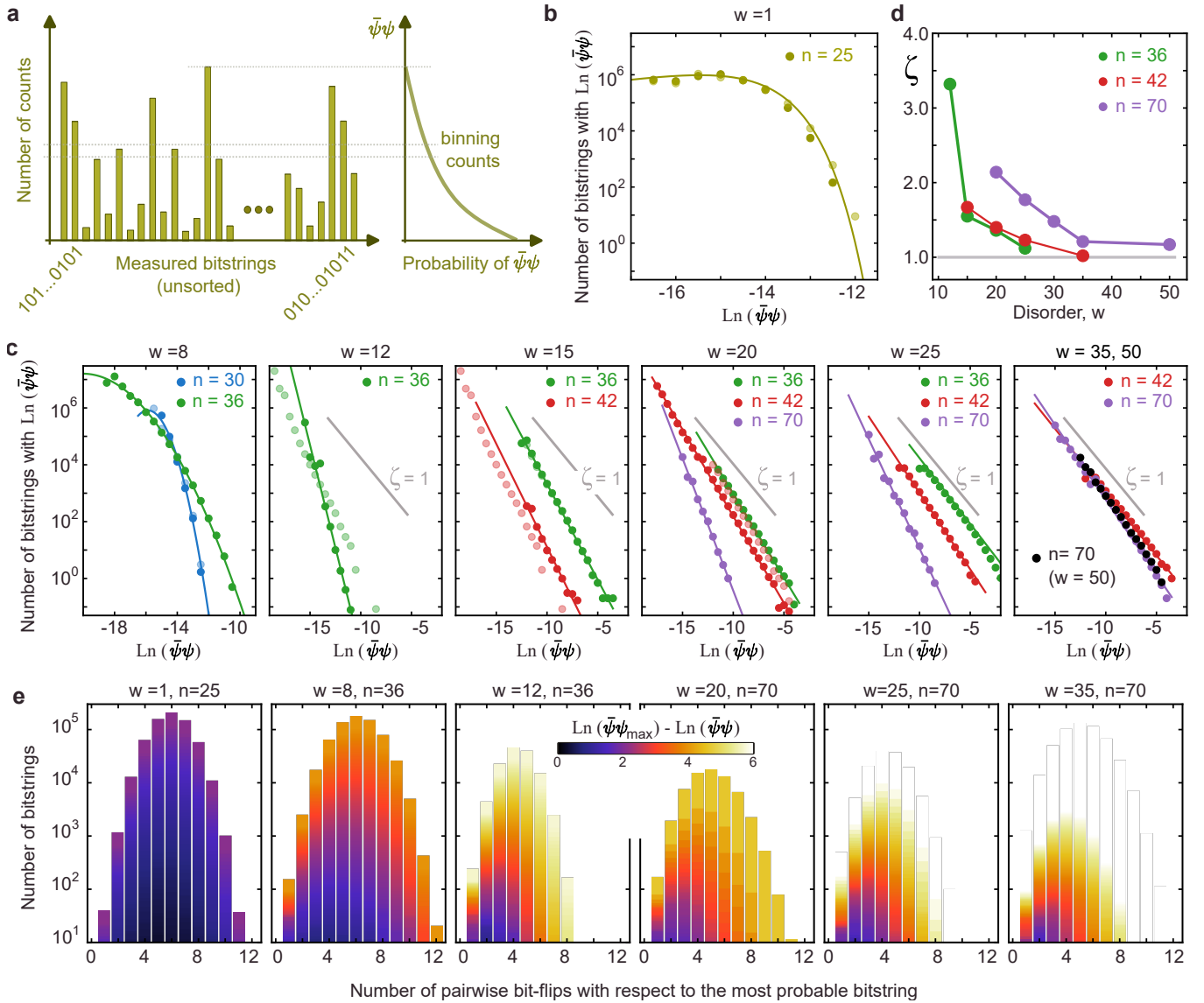


FIG. 5: Wavefunction statistics. **a**, We count the number of observations for each individual bitstring, allowing us to associate a quantum amplitude $\bar{\psi}\psi$ to the probability of measuring that specific bit-string. We then assemble these data into the probability distribution $\mathcal{P}(\bar{\psi}\psi)$. **b**, Unnormalized distribution as a function of $-\ln(\bar{\psi}\psi)$ for $n = 25$ at weak disorder, $w = 1$; line shows fit to the Porter-Thomas distribution. **c**, Left panel shows the data for slightly subcritical disorder, $w = 8$, plotted with quadratic fits (see main text) for $n = 30, 36$. Other panels show the evolution of $\mathcal{P}(\bar{\psi}\psi) \sim (\bar{\psi}\psi)^{-\zeta}$ with increasing disorder in the NEE phase. Solid and faded dots correspond to $Jt = 30$ and $Jt = 60$, respectively. Middle panels ($w = 12, 15, 20$) reveal that the distribution changes with time at weaker disorder $w = 12$ but is stationary for stronger disorder. Rightmost panel presents the data for the strongest disorder values ($w = 35, 50$) where ζ manifestly tends to 1 irrespective of size $n = 42, 70$. **d**, Evolution of the ζ exponent with increasing w in the glassy phase ($n = 36, 42, 70$). **e**, Spatial correlations of wavefunction intensities $\bar{\psi}\psi$ as a function of the number of bit-flips between them, together with the probability distribution $\mathcal{P}(\ln(\bar{\psi}\psi))$. Observe that upon increasing disorder, the number of actual bit-flips decreases (horizontal extent shrinks) while the probability distribution broadens (colour scale explores extremes).

from the short-time slope of the relaxation curve. Fig. 4b shows the fitted Γ versus the Laplacian eigenvalue, λ , for several disorder strengths and three different system sizes of 42, 59 and 70 qubits (50–100 disorder realizations for each case), which show good agreement for similar values

of λ . At low disorder, Γ scales linearly with the eigenvalue up to $\lambda \approx 0.5$, consistent with normal diffusion with diffusion constant \mathcal{D} . At stronger disorder, this proportionality weakens and eventually breaks down. Fig. 4c summarizes the extracted diffusion constant \mathcal{D} versus dis-

order strength, showing that near a critical value $w \simeq 10$, \mathcal{D} drops to $\mathcal{D} \sim 0.1$, while a finite residual magnetization M_∞ emerges for $w > w_c$. In this panel we also show the value of β resulting from fitting $\Gamma = a\lambda^\beta$; as expected, $\beta \approx 1$ in the ergodic phase but drops for $w > w_c$.

Statistics of wavefunctions in Hilbert space. To further study the effects of disorder on the behavior in Hilbert space, we next turn to the distribution of bitstring probabilities (Fig. 5a). Fully ergodic wavefunctions obey the Porter-Thomas [61] (PT) probability distribution, $\mathcal{P}_{PT}(N|\Psi|^2)$, where $\Psi \equiv \Psi[\sigma_i^z]$ is a many-body wavefunction in the σ_z basis; N is the Hilbert space dimension [62]; and $\mathcal{P}_{PT}(x) = \frac{1}{\sqrt{2\pi x}}e^{-x/2}$. We confirm that our data follow this distribution at low disorder, $w = 1$; see Fig. 5b. Increasing the disorder results in a qualitative change to the distribution $\mathcal{P}(N|\Psi|^2)$. Close to the glass transition, $w = 8$, the distribution broadens significantly and no longer obeys the Porter-Thomas fit; instead it becomes log-normal, as shown in the left panel of Fig. 5c. The data are fit to $\mathcal{P}_{MF}(y)dy$ with $y = \ln(x)$ and $\mathcal{P}_{MF}(y) \propto \exp(-a(y - y_m)^2)$, with fitting parameters $(a, y_m)_{n=30} = (1.1, -3.0)$ and $(a, y_m)_{n=36} = (0.185, -2.9)$. Such a distribution is known to exist in the context of mesoscopic fluctuations and (weak) Anderson localization [63–65]. At higher disorder, in the glassy phase, the distribution convincingly displays power-law behaviour—over 8 orders of magnitude in some cases. These data are shown in Fig. 5c, fit to $\mathcal{P}_{MF}(y) \sim e^{-\zeta y}$. Observe that the exponent ζ decreases steadily (see Fig. 5d) as a function of increasing w . At very strong disorder, $\zeta \rightarrow \zeta_\infty = 1$. This is in stark contrast to the localization transition on Random Regular Graphs [66], where $\zeta = 1/2$ at criticality and decreases further upon entering the localized phase. Anomalous behavior similar to our result with $\zeta_\infty = 1$ was found on Erdős-Rényi graphs [67], see also [68], hinting at its universality. The formation of anomalous distributions of wave functions in Hilbert space can be visualized if we plot the number of bitstrings as a function of Hilbert space distance from the wave function maximum (Fig 5e). The colour map corresponds to the relative probability of finding each constituent bitstring. In the ergodic state, one observes a rather flat (uniformly coloured) distribution of wave functions. This distribution becomes more peaked (stronger colour gradient) in the non-ergodic state, suggesting the formation of sharp spatial structures at high disorder in agreement with Ref. [67].

Quantum glass phases are particularly interesting from a computational perspective, as their non-universal dynamics challenge classical descriptions and require exponentially costly simulations. Ergodic states of quantum matter often exhibit a substantial degree of universality that depends only weakly on the specifics of the Hamiltonian, a property that frequently makes them more accessible to study via classical computational methods. MBL states—characterized by the existence of local integrals of motion (LIOMs)—have in some regimes been handled

using perturbative treatments starting from a fully frozen limit, making them more classically tractable [69]. The dynamics of a quantum system in a NEE phase, however, carry specific non-universal features tied to a particular disorder realization, thus limiting the efficacy of semi-classical Boltzmann approaches involving disorder averaging. Moreover, the NEE phase does not support LIOMs, which makes it more challenging to approach with convergent perturbative approaches based on MBL-like approximations. Direct quantum simulation is uniquely suited to the study of such systems, enabling extraction of key dynamical fingerprints and thereby a sensitive probe of the Hamiltonian parameters.

In this work, by characterizing the system in both Hilbert and real space, we found evidence for non-ergodic—though not fully localized—dynamics at high temperatures in a prototypical 2D disordered array of interacting spins. This behaviour spans a broad range of disorder strengths and serves as a high-temperature analogue of low- T spin glasses. The absence of spin diffusion in this glassy phase does not imply frozen energy transport. On the contrary, we expect energy to propagate throughout the phase via power-law decay, distinguishing it qualitatively from a fully localized MBL state. Our theoretical analysis (see Supplement) indicates that the glassy phase is characterized by a single-spin dephasing rate, Γ_ϕ , typically much larger than the relaxation rate, Γ_r —a likely generic feature of strongly disordered systems with local interactions. This dephasing slowly suppresses interferences and leads to irreversibility of the dynamics. At very strong disorder, the power-law exponent η of the return probability rapidly approaches zero for all accessible system sizes, suggesting a possible transition to a many-body-localized phase without transport. Similarly asymptotic behaviour is observed in the power-law exponent of the distribution over wavefunctions, ζ , which tends to one as the disorder is increased. These Hilbert space signatures are qualitatively distinct from what one might expect in the ergodic state, where the return probability is exponentially decaying and wavefunction statistics follow a Porter-Thomas distribution. Although we here consider system sizes of up to 70 qubits, this does not guarantee that we have reached the true asymptotic regime. The same holds for the accessible time window ($Jt \leq 100$). While these limitations prevent direct access to the strict thermodynamic limit, studies at these experimentally relevant scales already provide valuable insight into the physics of real quantum systems.

Acknowledgement Mikhail Feigel'man and Lev Ioffe are grateful to Vladimir Kravtsov for many useful discussions.

† Google Quantum AI and Collaborators

A. Lunkin^{1,‡}, N. S. Ticea^{2,3,‡}, S. Kumar^{2,4}, C. Miao^{2,5}, J. Choi^{2,6}, M. Alghadeer^{2,7}, I. Drozdov^{2,8}, D. Abanin², A. Abbas², R. Acharya², L. Aghababaei Beni², G. Aigeldinger², R. Alcaraz², S. Alcaraz², M. Ansmann², F. Arute², K. Arya², W. Askew², N. Astrakhantsev², J. Atalaya², R. Babbush², B. Ballard², J. C. Bardin^{2,9}, H. Bates², A. Bengtsson², M. Bigdeli Karimi², A. Bिल्mes², S. Bilodeau², F. Borjans², A. Bourassa², J. Bovaird², D. Bowers², L. Brill², P. Brooks², M. Broughton², D. A. Browne², B. Buchea², B. B. Buckley², T. Burger², B. Burkett², N. Bushnell², J. Busnaina², A. Cabrera², J. Campero², H.-S. Chang², S. Chen², Z. Chen², B. Chiaro², L.-Y. Chih², A. Y. Cleland², B. Cochrane², M. Cockrell², J. Cogan², R. Collins², P. Conner², H. Cook², R. G. Cortinas², W. Courtney², A. L. Crook², B. Curtin², M. Damyanov², S. Das², D. M. Debroy², S. Demura², P. Donohoe², A. Dunsworth², V. Ehimhen², A. Eickbusch², A. Moshe Elbag², L. Ella², M. Elzouka², D. Enriquez², C. Erickson², L. Faoro², V. S. Ferreira², M. Flores², L. Flores Burgos², S. Fontes², E. Forati², J. Ford², B. Foxen², M. Fukami², A. Wing Lun Fung², L. Fuste², S. Ganjam², G. Garcia², C. Garrick², R. Gasca², H. Gehring², R. Geiger², E. Genois², W. Giang², D. Gilboa², J. E. Goeters², E. C. Gonzales², R. Gosula², S. J. de Graaf², A. Grajales Dau², D. Graumann², J. Grebel², A. Greene², J. A. Gross², J. Guerrero², L. Le Guevel², T. Ha², S. Habegger², T. Hadick², A. Hadjikhani², M. C. Hamilton^{2,14}, M. Hansen², M. P. Harrigan², S. D. Harrington², J. Hartshorn², S. Heslin², P. Heu², O. Higgott², R. Hiltermann², J. Hilton², H.-Y. Huang², M. Hucka², C. Hudspeth², A. Huff², W. J. Huggins², E. Jeffrey², S. Jevons², Z. Jiang², X. Jin², C. Jones², C. Joshi², P. Juhas², A. Kabel², H. Kafri², H. Kang², K. Kang², A. H. Karamlou², R. Kaufman², K. Kechedzhi², J. Kelly², T. Khattar², M. Khezri², S. Kim², P. V. Klimov², C. M. Knaut², B. Kobrin², A. N. Korotkov², F. Kostritsa², J. M. Kreikebaum², R. Kudo², B. Kueffler², A. Kumar², V. D. Kurilovich², V. Kutsko², D. Landhuis², T. Lange-Dei², B. W. Langley², P. Laptev², K.-M. Lau², E. Leavell², J. Ledford², J. Lee², K. Lee², B. J. Lester², W. Leung², L. Li², W. Yan Li², M. Li², A. T. Lill², W. P. Livingston², M. T. Lloyd², L. De Lorenzo², E. Lucero², D. Lundahl², A. Lunt², S. Madhuk², A. Maiti², A. Maloney², S. Mandrà², L. S. Martin², O. Martin², E. Mascot², P. Masih Das², D. Maslov², M. Mathews², C. Maxfield², J. R. McClean², M. McEwen², S. Meeks², A. Megrant², K. C. Miao², Z. K. Mineev², R. Molavi², S. Molina², S. Montazeri², C. Neill², M. Newman², A. Nguyen², M. Nguyen², C.-H. Ni², M. Y. Niu², L. Oas², W. D. Oliver², R. Orosco², K. Ottosson², A. Pagano², A. Di Paolo², S. Peek², D. Peterson², A. Pizzuto², E. Portoles², R. Potter², O. Pritchard², M. Qian², C. Quintana², G. Ramachandran², A. Ranadive², M. J. Reagor², R. Resnick², D. M. Rhodes², D. Riley², G. Roberts², R. Rodriguez², E. Ropes², L. B. De Rose², E. Rosenberg², E. Rosenfeld², D. Rosenstock², E. Rossi², D. A. Rower², R. Salazar², K. Sankaragomathi², M. Can Sarihan², K. J. Satzinger², M. Schaefer^{2,10}, S. Schroeder², H. F. Schurkus², A. Shalingohar², M. J. Shearn², A. Shorter², V. Shvarts², V. Sivak², S. Small², W. Clarke Smith², D. A. Sobel², B. Spells², S. Springer², G. Sterling², J. Suchard², A. Szasz², A. Szein², M. Taylor², J. P. Thiruraman², D. Thor², D. Timucin², E. Tomita², A. Torres², M. Mert Torunbalci², H. Tran², A. Vaishnav², J. Vargas², S. Vdovichev², G. Vidal², B. Villalonga², C. Vollgraf Heidweiller², M. Voorhees², S. Waltman², J. Waltz², S. X. Wang², B. Ware², J. D. Watson², Y. Wei², T. Weidel², T. White², K. Wong², B. W. K. Woo², C. J. Wood², M. Woodson², C. Xing², Z. Jamie Yao², P. Yeh², B. Ying², J. Yoo², N. Yosri², E. Young², G. Young², A. Zalcman², R. Zhang², Y. Zhang², N. Zhu², N. Zobrist², Z. Zou², S. Boixo², H. Neven², V. Smelyanskiy², T. I. Andersen², P. Roushan², M. V. Feigel'man^{1,15,§}, L. B. Ioffe^{2,§}

1 Nanocenter CENN, Ljubljana, Slovenia

2 Google Research, Mountain View, CA, USA

3 Department of Applied Physics, Stanford University, Stanford, California 94305, USA

4 Department of Electrical and Computer Engineering, Princeton University, Princeton, NJ, USA

5 Department of Physics, Stanford University, Stanford California 94305, USA

6 School of Applied and Engineering Physics, Cornell University, Ithaca, New York 14853, USA

7 Department of Physics, Clarendon Laboratory, University of Oxford, OX1 3PU, UK

8 Department of Physics, University of Connecticut, Storrs, CT

9 Department of Electrical and Computer Engineering, University of Massachusetts, Amherst, MA

10 Department of Physics, University of California, Santa Barbara, CA

11 Department of Electrical and Computer Engineering, University of California, Riverside, CA

12 Pritzker School of Molecular Engineering, University of Chicago, Chicago, IL

13 Department of Physics and Astronomy, University of California, Riverside, CA

14 Department of Electrical and Computer Engineering, Auburn University, Auburn, AL

15 Jožef Stefan Institute, Ljubljana, Slovenia

‡ These authors contributed equally to this work.

§ Corresponding authors: Mikhail.Feigelman@nanocenter.si and ioffel@google.com

-
- [1] D. M. Basko, I. L. Aleiner, and B. L. Altshuler, Metal–insulator transition in a weakly interacting many-electron system with localized single-particle states, *Annals of Physics* **321**, 1126 (2006).
- [2] E. Altman and R. Vosk, Universal dynamics and renormalization in many-body-localized systems, *Annu. Rev. Condens. Matter Phys.* **6**, 383 (2015).
- [3] R. Nandkishore and D. A. Huse, Many-body localization and thermalization in quantum statistical mechanics, *Annu. Rev. Condens. Matter Phys.* **6**, 15 (2015).
- [4] D. J. Luitz and Y. B. Lev, The ergodic side of the many-body localization transition, *Annalen der Physik* **529**, 1600350 (2017).
- [5] F. Alet and N. Laflorencie, Many-body localization: An introduction and selected topics, *Comptes Rendus Physique* **19**, 498 (2018).
- [6] S. Gopalakrishnan and D. A. Huse, Instability of many-body localized systems as a phase transition in a non-standard thermodynamic limit, *Physical Review B* **99**, 134305 (2019).
- [7] D. A. Abanin *et al.*, Colloquium: Many-body localization, thermalization, and entanglement, *Rev. Mod. Phys.*

- 91**, 021001 (2019).
- [8] J. Suntajs, J. Bonča, T. Prosen, and L. Vidmar, Quantum chaos challenges many-body localization, *Physical Review E* **102**, 062144 (2020).
- [9] D. Sels and A. Polkovnikov, Dynamical obstruction to localization in a disordered spin chain, *Physical Review E* **104**, 054105 (2021).
- [10] J. C. Peacock and D. Sels, Many-body delocalization from embedded thermal inclusion, *Physical Review B* **108**, L020201 (2023).
- [11] P. Sierant, M. Lewenstein, A. Scardicchio, L. Vidmar, and J. Zakrzewski, Many-body localization in the age of classical computing, *Reports on Progress in Physics* **88**, 026502 (2025).
- [12] S. F. Edwards and P. W. Anderson, Theory of spin glasses, *Journal of Physics F: Metal Physics* **5**, 965 (1975).
- [13] K. Binder and A. P. Young, Spin glasses: Experimental facts, theoretical concepts, and open questions, *Reviews of Modern Physics* **58**, 801 (1986).
- [14] M. Mézard, G. Parisi, and M. A. Virasoro, *Spin Glass Theory and Beyond* (World Scientific, 1987).
- [15] J.-P. Bouchaud, L. F. Cugliandolo, J. Kurchan, and M. Mezard, "Out of Equilibrium dynamics in Spin-Glasses and other Glassy Systems", in "Spin Glasses and Random Fields", ed. A.P.Young, World Scientific (1998).
- [16] E. Vincent, "Ageing, Rejuvenation and Memory: The Example of Spin Glasses", in "Ageing and the Glass Transition", eds. M.Henkel, M.Pleimling and R.Sanctuary, Springer, Berlin Heidelberg (2009).
- [17] P. Esquinazi, *Tunneling systems in amorphous and crystalline solids* (Springer - Verlag, Berlin Heidelberg New York, 1998).
- [18] S. Kogan, *Electronic Noise and Fluctuations in Solids* (Cambridge University Press, 2008).
- [19] E. Paladino *et al.*, $1/f$ noise: implications for solid-state quantum information, *Rev. Mod. Phys.* **86**, 361 (2014).
- [20] P. Charbonneau, E. Marinari, G. Parisi, F. Ricci-Tersenghi, G. Sicuro, F. Zamponi, and M. Mezard, *Spin glass theory and far beyond: replica symmetry breaking after 40 years* (World Scientific, 2023).
- [21] W. De Roeck, L. Giacomin, F. Huveneers, and O. Prosnjak, Absence of normal heat conduction in strongly disordered interacting quantum chains, arXiv preprint arXiv:2408.04338 (2024).
- [22] J. Z. Imbrie, On many-body localization for quantum spin chains, *Journal of Statistical Physics* **163**, 998 (2016).
- [23] A. Pal and D. A. Huse, Many-body localization phase transition, *Physical Review B—Condensed Matter and Materials Physics* **82**, 174411 (2010).
- [24] E. V. Doggen *et al.*, Slow many-body delocalization beyond one dimension, *Phys. Rev. Lett.* **125**, 155701 (2020).
- [25] J. Li, A. Chan, and T. B. Wahl, Quantum circuits reproduce the experimental two-dimensional many-body localization transition point, *Phys. Rev. B* **109**, L140202 (2024).
- [26] J. Li, A. Chan, and T. B. Wahl, Two-dimensional many-body localized systems coupled to a heat bath, *Phys. Rev. B* **111**, 224211 (2025).
- [27] K. Tikhonov and A. Mirlin, Statistics of eigenstates near the localization transition on random regular graphs, *Physical Review B* **99**, 024202 (2019).
- [28] V. E. Kravtsov, I. M. Khaymovich, E. Cuevas, and M. Amini, A random matrix model with localization and ergodic transitions, *New J. Phys.* **17**, 122002 (2015).
- [29] G. D. Tomasi *et al.*, Survival probability in generalized rosenzweig-porter random matrix ensemble, *SciPost Physics* **6**, 014 (2019).
- [30] G. Biroli and M. Tarzia, Fractal and nonergodic phases in random matrix models, *Phys. Rev. B* **103**, 104205 (2021).
- [31] A. V. Lunkin and K. Tikhonov, Local density of states correlations in the Lévy-Rosenzweig-Porter random matrix ensemble, *SciPost Physics* **19**, 015 (2025).
- [32] E. Safonova, A. Lunkin, and M. Feigel'man, Density of states correlations in Lévy Rosenzweig-Porter model via supersymmetry approach, *SciPost Phys.* **20**, 003 (2026).
- [33] L. Faoro, M. V. Feigelman, and L. Ioffe, Non-ergodic extended phase of the quantum random energy model, *Ann. Phys.* **409**, 167916 (2019).
- [34] V. N. Smelyanskiy *et al.*, Nonergodic delocalized states for efficient population transfer within a narrow band of the energy landscape, *Phys. Rev. X* **10**, 011017 (2020).
- [35] M. Winer *et al.*, Spectral form factor of a quantum spin glass, *J. High Energy Phys.* **2022**, 32.
- [36] M. Mezard and A. Montanari, *Information, physics, and computation* (Oxford University Press, 2009).
- [37] Y. B. Lev *et al.*, Absence of diffusion in an interacting system of spinless fermions on a one-dimensional disordered lattice, *Phys. Rev. Lett.* **114**, 100601 (2015).
- [38] K. Agarwal *et al.*, Anomalous diffusion and griffiths effects near the many-body localization transition, *Phys. Rev. Lett.* **114**, 160401 (2015).
- [39] N. Macé, F. Alet, and N. Laflorencie, Multifractal scalings across the many-body localization transition, *Phys. Rev. Lett.* **123**, 180601 (2019).
- [40] M. Pino *et al.*, Nonergodic metallic and insulating phases of josephson junction chains, *Proc. Natl. Acad. Sci. U.S.A.* **113**, 536 (2016).
- [41] M. Pino, V. Kravtsov, B. Altshuler, and L. Ioffe, Multifractal metal in a disordered josephson junctions array, *Physical Review B* **96**, 214205 (2017).
- [42] D. M. Long, P. J. D. Crowley, V. Khemani, and A. Chandran, Phenomenology of the prethermal many-body localized regime, *Phys. Rev. Lett.* **131**, 106301 (2023).
- [43] M. Tarzia, Many-body localization transition in hilbert space, *Phys. Rev. B* **102**, 014208 (2020).
- [44] G. Biroli *et al.*, Large-deviation analysis of rare resonances for the many-body localization transition, *Phys. Rev. B* **110**, 014205 (2024).
- [45] T. Thiery *et al.*, Many-body delocalization as a quantum avalanche, *Phys. Rev. Lett.* **121**, 140601 (2018).
- [46] W. D. Roeck and F. Huveneers, Stability and instability towards delocalization in many-body localization systems, *Phys. Rev. B* **95**, 155129 (2017).
- [47] S. Gopalakrishnan *et al.*, Griffiths effects and slow dynamics in nearly many-body localized systems, *Phys. Rev. B* **93**, 134206 (2016).
- [48] E. Altman *et al.*, Quantum simulators: Architectures and opportunities, *PRX Quantum* **2**, 017003 (2021).
- [49] M. Schreiber *et al.*, Observation of many-body localization of interacting fermions in a quasirandom optical lattice, *Science* **349**, 842 (2015).
- [50] J.-y. Choi, S. Hild, J. Zeiher, P. Schauss, A. Rubio-Abadal, T. Yefsah, V. Khemani, D. Huse, I. Bloch, and C. Gross, Exploring the many-body localization transition in two dimensions, *Science* **352**, 1547 (2016).

- [51] P. Bordia *et al.*, Periodically driving a many-body localized quantum system, *Nature Physics* **13**, 460 (2017).
- [52] T.-M. Li *et al.*, Many-body delocalization with a two-dimensional 70-qubit superconducting quantum simulator, arXiv preprint arXiv:2507.16882 (2025).
- [53] J. Hur *et al.*, Stability of many-body localization in two dimensions, arXiv preprint arXiv:2508.20699 (2025).
- [54] M. Kjaergaard, M. E. Schwartz, J. Braumüller, P. Krantz, J. I.-J. Wang, S. Gustavsson, and W. D. Oliver, Superconducting qubits: Current state of play, *Annual Review of Condensed Matter Physics* **11**, 369 (2020).
- [55] J. P. A. Zúniga *et al.*, Critical properties of the superfluid - boseglass transition in two dimensions, *Phys. Rev. Lett.* **114**, 155301 (2015).
- [56] L. Leviandier *et al.*, Fourier transform: A tool to measure statistical level properties in very complex spectra, *Phys. Rev. Lett.* **56**, 2449 (1986).
- [57] E. J. Torres-Herrera *et al.*, Generic dynamical features of quenched interacting quantum systems: Survival probability, density imbalance, and out-of-time-ordered correlator, *Phys. Rev. B* **97**, 060303(R) (2018).
- [58] E. J. Torres-Herrera and L. F. Santos, Dynamics at the many-body localization transition, *Phys. Rev. B* **92**, 014208 (2016).
- [59] M. Hopjan and L. Vidmar, Scale-invariant survival probability at eigenstate transitions, *Phys. Rev. Lett.* **131**, 060404 (2023).
- [60] M. Hopjan and L. Vidmar, Scale-invariant critical dynamics at eigenstate transitions, *Phys. Rev. Res.* **5**, 043301 (2023).
- [61] C. E. Porter and R. G. Thomas, Fluctuations of nuclear reaction widths, *Phys. Rev.* **104**, 483 (1956).
- [62] Since our dynamics conserves total spin projection $S_{tot}^z = 0$, the Hilbert space dimension is equal to $N = n! / (\frac{n}{2}!)^2$.
- [63] B. Altshuler, V. Kravtsov, and I. Lerner, Statistics of mesoscopic fluctuations and instability of one-parameter scaling, *Sov.Phys.-JETP* **64**, 1352 (1986).
- [64] V. I. Fal'ko and K. B. Efetov, Statistics of prelocalized states in disordered conductors, *Phys. Rev. B* **52**, 17413 (1995).
- [65] A. Mirlin and F. Evers, Anderson transitions, *Rev. Mod. Phys.* **80**, 1355 (2008).
- [66] A. De Luca, B. L. Altshuler, V. E. Kravtsov, and A. Scardicchio, Anderson localization on the bethe lattice: Nonergodicity of extended states, *Phys. Rev. Lett.* **113**, 046806 (2014).
- [67] L. F. Cugliandolo, G. Schehr, M. Tarzia, and D. Venturelli, Multifractal phase in the weighted adjacency matrices of random erdős-rényi graphs, *Phys. Rev. B* **110**, 174202 (2024).
- [68] A. De Luca, B. L. Altshuler, V. E. Kravtsov, and A. Scardicchio, Support set of random wavefunctions on the bethe lattice, arXiv preprint (2014), arXiv:1401.0019.
- [69] J. H. Bardarson, F. Pollmann, and J. E. Moore, Unbounded growth of entanglement in models of many-body localization, *Phys. Rev. Lett.* **109**, 017202 (2012).
- [70] Google Quantum AI, Quantum error correction below the surface code threshold, *Nature* **638**, 920 (2025).
- [71] T. I. Andersen, N. Astrakhantsev, A. H. Karamlou, J. Berndtsson, J. Motruk, A. Szasz, J. A. Gross, A. Schuckert, T. Westerhout, Y. Zhang, *et al.*, Thermalization and criticality on an analogue-digital quantum simulator, *Nature* **638**, 79 (2025).
- [72] W. A. Phillips, Two-level states in glasses, *Reports on Progress in Physics* **50**, 1657 (1987).
- [73] D. B. Gutman *et al.*, Energy transport in the anderson insulator, *Phys. Rev. B* **93**, 245427 (2016).
- [74] L. Faoro and L. B. Ioffe, Internal loss of superconducting resonators induced by interacting two-level systems, *Phys. Rev. Lett.* **109**, 157005 (2012).
- [75] V. K. Varma *et al.*, Energy diffusion in the ergodic phase of a many-body localizable spin chain, *J. Stat. Mech.* , 053101 (2017).
- [76] J. Herbrych and P. Prelovsek, Spin and energy diffusion versus subdiffusion in disordered spin chains, *Phys. Rev. B* **112**, 045108 (2025).
- [77] M. V. Feigel'man, L. B. Ioffe, and M. Mézard, Superconductor-insulator transition and energy localization, *Phys. Rev. B* **82**, 184534 (2010).
- [78] R. Abou-Chakra, D. J. Thouless, and P. W. Anderson, A self-consistent theory of localization, *J. Phys. C* **6**, 1734 (1973).
- [79] V. E. Kravtsov, B. L. Altshuler, and L. B. Ioffe, Non-ergodic extended states in disordered systems, *Ann. Phys.* **389**, 148 (2018).
- [80] B. Derrida and H. Spohn, *Journal of Statistical Physics* **51**, 817 (1988).
- [81] B. Derrida, *Physica A* **163**, 71 (1990).
- [82] G. Biroli, G. Semerjian, and M. Tarzia, *Progress of Theoretical Physics Supplement* **184**, 187 (2010).

CONTENTS

References	8
1. List of symbols	12
2. Experimental details	13
2.A. Procedure	13
2.B. Data fitting	13
3. Qualitative theoretical description	14
3.A. Short time dynamics of return probability	14
3.B. $1/f$ spin noise	14
3.C. Exponent η and its n -dependence.	15
3.D. Dephasing without relaxation: results of a model calculation	16
4. Recursion relations for spin- $\frac{1}{2}$ model on the Cayley tree	17
4.A. Preliminaries	17
4.B. Recursion equations for the relaxation rates	18
4.C. Calculation of dephasing rates	18
a. Schrieffer - Wolff transformation	18
b. Recursion equations for dephasing	19
5. Thresholds for the relaxation and dephasing channels	20
5.A. "Upper limit" approximation	20
a. Relaxation rate	20
b. Dephasing rate	20
5.B. Account for self-energy correction	21
a. Relaxation rate threshold	21
b. Dephasing rate threshold	21

1. LIST OF SYMBOLS

Symbol	Description
J	Spin-spin coupling strength (XY interaction)
H	Hamiltonian of the spin- $\frac{1}{2}$ model on the Cayley tree
σ_i^a	Pauli matrices (where $a = x, y, z$ or $1, 2, 3$), $\sigma_i^a = 2S_i^a$
σ_i^\pm	Raising and lowering spin operators, S_i^\pm
h_i	Random magnetic field at site i
W	Full width of the box distribution for h_i
n	Total number of spins (or system size)
K	Branching number of the Cayley tree (CT)
Z	Full coordination number of sites on CT, $Z = K + 1$
\mathcal{H}	Operator $\hat{1} \otimes H^T - H \otimes \hat{1}$ in the extended Hilbert space
$ \hat{O}\rangle$	Operator \hat{O} represented as a wave function in the extended space
\mathcal{V}	Perturbation operator in the extended space, related to V
Γ_i^r, Γ_j^\pm	Local relaxation rate for spin at site i (or j)
$\Sigma_z(\epsilon)$	Self-energy for the z -component of spin operator
$\Sigma_\pm(\epsilon)$	Self-energy for the σ^\pm components
U	Anti-hermitian operator for Schrieffer - Wolff transformation
H_{eff}	Effective Hamiltonian after Schrieffer - Wolff transformation
V_{eff}	Effective perturbation Hamiltonian, $\frac{1}{2}[V, U]$
Γ_j^ϕ	Local dephasing rate for spin at site j
J_r, j_r	Critical coupling strength and dimensionless ratio ($j_r = J_r/W$) for relaxation
J_ϕ, j_c	Critical coupling strength and dimensionless ratio ($j_c = J_\phi/W$) for dephasing
$F(x)$	Function used to determine the critical point of linear recursions
$P_0(h)$	Bare distribution function for the local field h
$P_1(h)$	Effective distribution function for h accounting for self-energy correction (relaxation)
$P_2(h_1, h_2)$	Renormalized distribution function for h_1, h_2 (dephasing)
$G(e^{-x})$	Laplace transform of the probability density function $\mathcal{P}(\Gamma_j)$
S	$\text{Re } \Sigma$, the real part of the self-energy correction (dephasing)

2. EXPERIMENTAL DETAILS

2.A. Procedure

The experiments were performed on a Willow device architecture as presented in Ref. [70], using the calibration protocols shown in Ref. [71] to set the coupling rates and Z -fields of the analog Hamiltonian. Since the Hamiltonian is photon number conserving, we mitigate the effects of photon loss by postselecting the data, removing any bitstrings in which the photon number is not conserved.

In all experiments, the qubit frequencies are first ramped quickly (~ 1 ns) to the values corresponding to the relevant disorder instance, before ramping up the coupling rates over another ~ 1 ns. The system is then evolved for a variable amount of time under the analog Hamiltonian, followed by a 1 ns Hamiltonian off-ramp, and finally measurements in the Z -basis.

2.B. Data fitting

As discussed in the main text, the dependence of Edwards-Anderson order parameter on time fits well the power law, $C_{fit}(t) = at^{-\alpha}$ at low $w < w_c \approx 10$ and fits well exponential law at $w > w_c$ with non-zero offset: $C_{fit}(t) = a \exp(-\Gamma t) + Q_{EA}$ or $C_{fit}(t) = at^{-\alpha} \exp(-\Gamma t) + Q_{EA}$ close to the transition. This statement can be made more quantitative if we compare the actual data with the fits and define quality of fit, χ by

$$\chi = \frac{1}{n_t} \sum_t \left(\frac{C_{fit}(t) - C_t}{C_t} \right)^2 \quad (S6)$$

where n_t is the number of data points in time, $C_{fit}(t)$ is the fitting function and C_t is filtered value of measured magnetization squared after time t , $m_t^2 = (1/n) \sum_i \langle \sigma_i^z(t) \rangle^2$. The measured values of m_t^2 fluctuates significantly over time, even after being averaged over 100 realizations. These fluctuations dominate the fit quality χ at large disorders; to suppress this effect, we smoothed the data by applying the Savitsky Golay filter, G_r , with degree $r = 2 - 5$ to the data: $C_t = \sum_{t'} G_r(t - t') m_{t'}^2$. We emphasize that the fit parameters are not affected by the application of the filter; it affects only the evaluation of the fit quality, χ . Slightly above the transition the best fit is achieved by an exponential with a power law prefactor and constant offset, see Fig.S6a. Below the transition, at $w < w_c \sim 10$, the power law fit is preferred, see Fig.S6b. Similarly, exponential fits with constant offset are poor below the transition. Far above the transition, exponential and exponential with power law prefactor fits perform equally well. In this regime, the exponent α of the power law becomes very small, e.g. $\alpha = 0.15$ for $w = 20$, which makes it very difficult to distinguish the fits. The values of the constant offset for these two fits are practically identical above the transition.

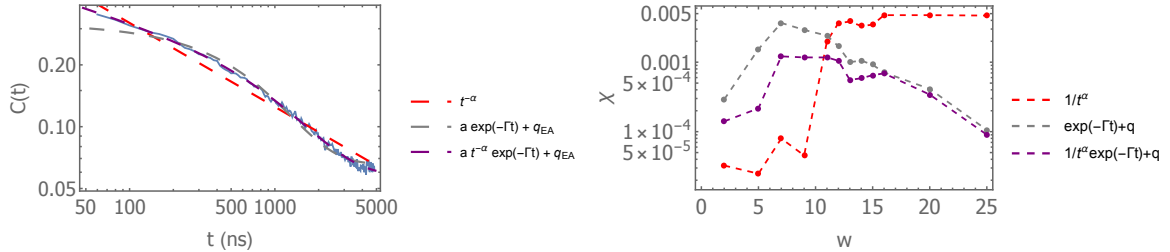


FIG. S6: Comparison of remanent magnetization fits by different time dependencies. Left panel: data for $n = 59$ $w = 14$ and their fits, with and without offset. The data shown here were filtered with a degree $r = 2$ Savitsky Golay filter. Right panel: data deviation from different fits as a function of w for $n = 59$. Below the phase transition, the power law fit is preferred, while above the transition, the exponential-with-constant-offset fit dominates. One cannot distinguish between a pure exponential fit and the fit for an exponential with a power law prefactor.

3. QUALITATIVE THEORETICAL DESCRIPTION

3.A. Short time dynamics of return probability

The short time behavior of $R(t)$ at $Jt \leq 1$ is well-described by the simplest approximation of independent spin pairs defined by the Hamiltonian:

$$H_0 = \sum_{\mu} H_{\mu} = \sum_{\mu} [J\tau_{\mu}^x + \varepsilon_{\mu}\tau_{\mu}^z] \quad (\text{S7})$$

where τ_{μ} denote Pauli matrices of combined spin operators on the links: $\tau_{\mu}^x = S_r^+ S_{r'}^- + h.c.$, $\tau_{\mu}^z = S_r^z - S_{r'}^z$, while $\mu \equiv \langle r, r' \rangle$ is defined on each lattice bond and $\varepsilon_{\mu} \equiv \varepsilon_{r,r'} = \frac{1}{2}(h_r - h_{r'})$. The meaning of approximation (S7) is to account for spin-flip events that occur at each link μ in the lowest order over coupling J ; here we mean, in terms of original spins S_r , a projection of the two-spin Hilbert space (dimension 4) to the subspace $|\uparrow\downarrow\rangle, |\downarrow\uparrow\rangle$ only. From this Hamiltonian, one can calculate the return probability as a function of time. Because all spin flips are independent in this approximation, we solve for the dynamics of each pair, find the return probability for this pair and take a product over all pairs:

$$R(t) = \prod_{\langle r, r' \rangle} \left[1 - \frac{J^2}{\varepsilon_{r,r'}^2 + J^2} \sin^2 \left(t \sqrt{\varepsilon_{r,r'}^2 + J^2} \right) \right] \quad (\text{S8})$$

where the product goes over all $2n$ pairs of nearest neighbors, here τ_{μ} defined on each lattice bond $\langle r, r' \rangle \equiv \mu$. This approximation is good for $Jt \leq 1$, as one can observe from comparing the corresponding data in Fig. S7 with the calculation based on the Hamiltonian (S7), see below. $R(t)$ defined by Eq.(S8) is a random quantity that depends on specific realization of h_r . Representative $R(t)$ can be obtained by the averaging of $\ln R(t)$ over h_r , since this is an additive quantity: $R_{typ}(t) = \exp\{\overline{\ln R(t)}\}$, where $\overline{[\dots]}$ denotes averaging over independent random h_r . Approximation of independent pairs (S8) leads to a finite disorder-dependent limit for $R_{typ}(\infty)$ that can be calculated as

$$-\ln R_{typ}(\infty) \approx m \frac{4(\pi - 2)}{w} \quad (\text{S9})$$

The $m \leq n$ factor counts the number of bonds on a square lattice with n sites and with $h_r h_{r'} < 0$, and the integral over the distribution of $\varepsilon_{r,r'}$ is calculated to leading order in $1/w \ll 1$.

We numerically evaluate the expression for $R_{typ}(t)$ at $w = 15$, plotting the results in Fig. S7a by a blue dashed line (for $n = 25$) and a grey dashed line, $n = 36$. Results of direct numerical simulation of $R_{typ}(t)$ for $n = 16, 20$ and two instances of $n = 25$ are shown by full lines, together with experimental data for $n = 36$. Good agreement between approximation (S8) and the data is seen until $Jt \approx 1$ corresponding to $t \approx 30$ ns, while at later time-scales qualitative deviations occur. Indeed, while the theoretical dashed curves shows damped oscillations approaching a constant value at $t \rightarrow \infty$, the data (in brown) demonstrate faster decay of the oscillation amplitude and overall downshift of $R(t)$, in agreement with Eq.(2) of the Main text. We will argue below that such a behavior is due to residual interaction between different spin pairs τ_{μ}, τ_{ν} leading to dephasing and inelastic transitions.

Power-law behavior at long times means that the probability of flipping any spin S_r in the array grows logarithmically with time like $P_{\text{flip}} \sim (\eta/n) \ln(Jt)$; such behavior is akin to spin noise with $1/f$ power spectrum, known to be generic for glasses and spin glasses. Indeed, numerical simulations (see next Subsection) demonstrate a spin noise spectrum $\mathcal{S}(\omega) = \langle |S_r^z(\omega)|^2 \rangle \approx \frac{A}{|\omega|}$.

3.B. $1/f$ spin noise

Slow relaxation in glasses or spin glasses is usually associated with the presence of a broad spectrum $P(\Gamma)d\Gamma$ of relaxation rates Γ that characterize the dynamics of various modes of fluctuations, commonly known as two-level systems. If a broad distribution, $P(\Gamma)d\Gamma \sim d\Gamma/\Gamma$, is assumed, one immediately arrives [19] at the prediction of the noise spectrum $\mathcal{S}(\omega) \propto 1/|\omega|$. To check if such noise is present in our system, we performed numerical simulation of the dynamics described by (1) for system size $n = 20$. We computed local spin-spin correlation functions $S_r(t) = \langle S_r^z(0)S_r^z(t) \rangle$ and then averaged over positions \mathbf{r} and realizations of disorder to obtain $S(t) = \overline{\langle S_r^z(0)S_r^z(t) \rangle}$. Its Fourier transform $\mathcal{S}(\omega)$ is plotted in Fig. S7b. One observes $1/f$ noise over two decades in frequency.

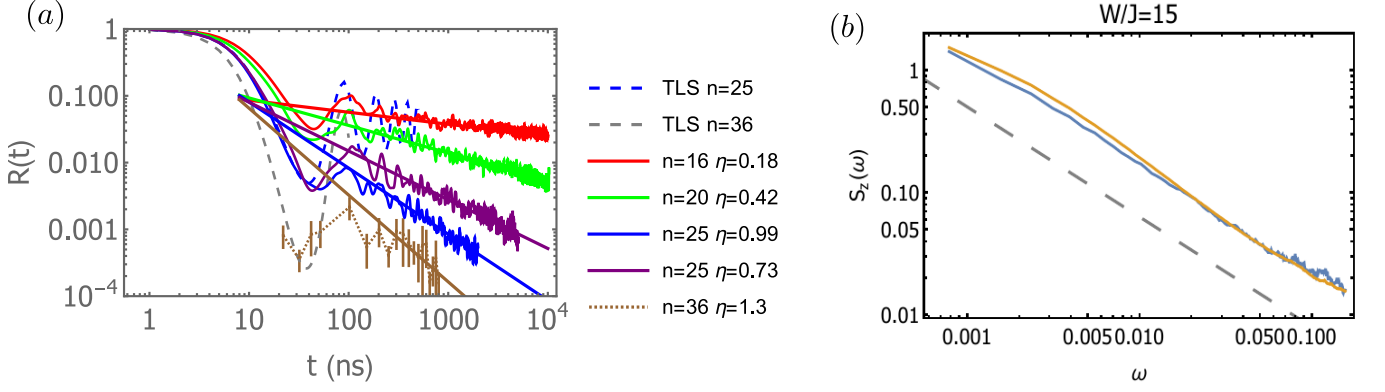


FIG. S7: Panel a): Return probability $R(t)$ for moderate disorder $w = 15$; dashed lines obtained with model Hamiltonian (S7), full lines numerically for $n = 16, 20, 25$, dotted line is for experimental data for $n = 36$. Panel b): Power spectrum of local spin $S^z(t)$ fluctuations: numerical simulation on the system of $n = 20$ spins with $w = 15$.

3.C. Exponent η and its n -dependence.

To explain the power-law decay of $R(t)$ with exponent $\eta \propto n^2$, we refer to the phenomenology of two-level systems in glasses [72] and to the related mechanism of $1/f$ noise [19]. The key point is the existence of a broad spectrum of very low frequencies in a system. The toy Hamiltonian described earlier (S7) is not sufficient in that respect, since all its eigenvalues are $\geq J$. Thus it is natural to take into account the interactions between effective spins τ_μ , which makes possible correlated flips of pairs of spins such that there is a small change in the total energy of a pair, see e.g. [73, 74]. Notice that the scaling described by (4)[Main text] cannot be valid at arbitrary large $n \rightarrow \infty$ since at any fixed large Jt it would make $R(t)$ smaller than the minimal IPR value $I_2^{\min} = 2^{-n}$. However, due to the smallness of $\kappa(w) \leq 1/w^2$, [see Eq.(5) of the Main text], the upper bound $n_{\max} \geq w^2$ compatible with such a dependence exceeds the maximal size of our system, even for critical disorder $w \approx w_r$. Thus our results for $\eta(n)$ dependence refer to the intermediate asymptotics of *moderately large* systems with $1 \ll n \leq n_{\max}(w)$.

Moving forward, it will be sufficient to consider only the spins satisfying $|\epsilon_\mu| \leq J$ —we will call them “coherent TLS”. Assuming uniformly distributed disorder, the fraction of these spins is $\sim 2/w \ll 1$. The interaction Hamiltonian between these pairs is given by

$$H_{\text{int}} = \frac{1}{2} \sum_{\mu\nu} V_{\mu,\nu} (\tau_\mu^+ \tau_\nu^- + h.c.) \quad (\text{S10})$$

so that the full Hamiltonian consists of Eqs.(S7,S10). The total number of effective spins participating in the dynamics, therefore, is approximately $n_* = 2n \times (2/w) \gg 1$. Matrix elements $V_{\mu,\nu}$ appear in higher orders of perturbation theory as powers of $j = 1/w \ll 1$: these represent interactions between rare active TLS’s via the “inert media” of all other spins. Therefore, $V_{\mu,\nu}$ are mostly small compared to J , and the statistical distribution of their absolute values is very broad. Writing $|V_{\mu,\nu}| = J \exp(-L_{\mu,\nu})$ we present this distribution via

$$\mathcal{P}(L) dL \approx P_1 dL \quad \text{where} \quad L_{\min} < L < L_{\max} \quad (\text{S11})$$

with $L_{\min} \sim \ln w$ and $L_{\max} \sim n_* \ln w \gg L_{\min}$.

Now we formulate the key assumption of the further theoretical analysis: the system of interacting TLS’s is characterized (for values of w corresponding to the glassy state) by a dephasing rate Γ_ϕ that is much larger than the relaxation rate Γ . Theoretical arguments demonstrating the possibility of such a situation are provided in Secs. 4 and 5 below. Qualitatively, spin dephasing without spin relaxation is equivalent to the presence of energy transport in the absence of full ergodicity; low-temperature glasses provide a useful example of such a situation. Indeed, dephasing-only is present as soon as the effective magnetic field h_r^z acting at a site r acquires a slow time dependence due to the coupling of \mathbf{S}_r to other spins. Since the total energy of the system is conserved, this is possible if energy transport is allowed between different parts of the system. Within the MBL framework, studies of energy transport were provided in Ref. [75, 76].

We expect $\Gamma_\phi \ll J$ but still larger than most of the matrix elements $V_{\mu,\nu}$ since the latter are due to high-order processes. Then *real transitions* leading both to $1/f$ noise and to logarithmic growth of $-\ln R(t)$ occur due to the

interaction (S10) between pairs of active TLS with small $|E_\mu - E_\nu|$, where $E_\mu = \sqrt{\varepsilon_\mu^2 + J^2}$ is the energy splitting for the non-interacting model. An estimate for the rate $r_{\mu\nu}$ of such (incoherent) transition is given by $r_{\mu\nu} \sim V_{\mu,\nu}^2 \Gamma_\phi / |E_\mu - E_\nu|^2$ (compare with Eq.(26) from Ref. [19]). Exponentially broad distribution of matrix elements $V_{\mu,\nu}$ defined by Eq.(S11) translates then to the same kind of distribution for the rates $r_{\mu\nu} \sim \Gamma_\phi e^{-2L_{\mu\nu}}$. Factor P_1 in Eq.(S11) is proportional to n due to the normalization condition $\int \mathcal{P}(L)dL = P_1 L_{\max} \propto n_*^2$ since total number of pairs of interacting TLS scales as n_*^2 , and also $L_{\max} \propto n_*$. In result, we find that $P_1 = \gamma n$ where $\gamma \equiv \gamma(w)$.

Probability for any spin to be involved in inelastic relaxation during long time $t \gg 1/J$ grows $\propto \gamma n \ln(Jt)$. Now, in order to obtain the estimate for the full probability of return $R(t)$, one needs to take into account that $\ln R(t)$ is additive over all spins, thus an additional multiplication on the number of spins n should be performed. This way one gets power-law decay, $R_{\text{typ}}(t) \sim (Jt)^{-\eta}$, with exponent $\eta \propto n^2$, not far from its experimentally observed dependence in Eq.(3) of the Main text.

3.D. Dephasing without relaxation: results of a model calculation

Our analysis provided above that explains power-law dependence $R(t) \sim 1/t^\eta$ with for $\eta(n) \propto n^2$, is based on the assumption of dephasing rate Γ^ϕ being much higher than rate of inelastic relaxation Γ^r . In fact, we assumed that non-zero $\Gamma^\phi > 0$ is generated at $j_c < J/W \ll 1$ once original couplings J between neighboring spins in the Hamiltonian (1) [Main text] are taken into account, while for relaxation (real spin flips) an analogous critical value $j_r = J_r/W$ is larger, $j_r > j_c$. In such a case at $j_c < J/W < j_r$ relaxation processes are due to high-order terms of the J/W expansion, thus the inequality $\Gamma^r \ll \Gamma^\phi$ holds. Below in Sec.4 we present a calculation for the Hamiltonian (1) of the Main text, but living on the Cayley tree with branching number $K \gg 1$, which demonstrates $j_c \ll j_r$. Here in this Subsection we provide a brief account of that calculation, concentrating on its main results.

We define Γ^ϕ as $\text{Im } \Sigma^\pm$ where $\Sigma^\pm(\omega)$ is the self-energy part corresponding to transverse spin Green function $G^\pm(\omega)$; similarly, relaxation rate Γ^r is defined via self-energy of longitudinal Green function $G^{zz}(\omega)$. Using Heisenberg equations for spin operators and using the absence of loops on Cayley tree, one can derive (see next Sec.4) recursion relations for local relaxation rates Γ_i^r , similar (but different) to those of Ref.[77]:

$$\Gamma_0^r = J^2 \sum_j \frac{\Gamma_j^r}{(h_j - h_0)^2} \quad (\text{S12})$$

Summation here goes over K neighbors of the "central spin" \mathbf{S}_0 . Below we use bare distribution of local energies $P_0(h) = \frac{1}{W} \theta(W/2 - |h|)$. Recursions (S12) converge under iterations to $\Gamma^r = 0$ at $J < J_r$ while at larger J linear iterations diverge and nonlinear in Γ^r terms are needed to get a final nonzero result. Next, we assume $J < J_r$ and derive (in the next order over J^2) analogous equations for Γ^ϕ :

$$\Gamma_0^\phi = J^4 \sum_{j \neq k} \left(\frac{1}{h_0 - h_j} + \frac{1}{h_0 - h_k} \right)^2 \frac{\Gamma_j^\phi + \Gamma_k^\phi}{(h_j - h_k)^2} \quad (\text{S13})$$

Summation goes over $K(K-1)/2$ pairs of unequal neighbors of the site 0. Eqs.(S13) can be used to determine the boundary of the parameter region where non-zero Γ^ϕ are generated, that is $J_c = J_c(K)$. In general, equations for Γ^ϕ contain also terms of order J^2 , but these terms are inefficient at $J < J_r$ and thus omitted here.

At very small J/W we can neglect correlations between Γ_i^r at some site i and local field h_i ; it amounts to setting $h_0 = 0$ in Eq.(S12). Then these equations become identical to those derived in Ref. [78] for Anderson localization on a tree (of branching number K), within simplest "upper limit" approximation that neglects level repulsion (that is, real part of self-energy). Then critical value $j_r = J_r/W$ obeys simple equation $(2j_r)^{-1} = eK |\ln(2j_r)|$. Its solution for $K = 3$ is $j_r \approx 1.86 \cdot 10^{-2}$. Generalizing the same procedure for recursion equations (S13), one can find (see Sec. 5 below) the critical value $j_c = J_c/W$ within "upper limit approximation" equal to $j_c = 1.5 \cdot 10^{-2}$, thus confirming that $j_c < j_r$. The same inequality survives for larger values of K .

One can make a better calculation for both j_r and j_c taking into account corrections to the real part of self-energy function. For Eq.(S12) we can follow closely the approach proposed in Ref. [79] and get $j_r = 0.03$ for $K = 3$. Generalization of the same approach to the case of recursions (S13) is provided in Sec.5 below and leads to $j_c = 0.02$ at $K = 3$. The ratio $j_r/j_c \approx 1.5$ was found for larger values of K as well. We conclude that various approximation schemes consistently support our qualitative picture: in some range of W values the single-spin dephasing rate is much stronger than its relaxation rate.

4. RECURSION RELATIONS FOR SPIN- $\frac{1}{2}$ MODEL ON THE CAYLEY TREE

The main goal of the theory developed below is to demonstrate that local nature of spin-spin interaction in a random system may lead to the situation when local spin dephasing time is typically much shorter than spin relaxation time. To show it, as a matter of principle, we will use drastic simplification of our problem; namely, we consider spins $\frac{1}{2}$ sitting on a Cayley tree (infinite Bethe lattice) instead of a real square lattice.

4.A. Preliminaries

We are going to study a system of spins- $\frac{1}{2}$ in a random magnetic field with XY interaction on a Cayley tree (CT) with large branching number $K \gg 1$. The Hamiltonian is of the following form:

$$H = -J \sum_{\langle i,j \rangle} (\sigma_i^+ \sigma_j^- + \sigma_j^+ \sigma_i^-) + \frac{1}{2} \sum_i h_i \sigma_i^z. \quad (\text{S14})$$

where i, j are sites the Cayley tree, summation in the first term goes over links $\langle i, j \rangle$ of nearest neighbours. Random variables h_i belong to uncorrelated symmetric box distribution of full width W . Operators $\sigma_i^a = 2S_i^a$ with $a = 1, 2, 3$ are Pauli matrices, while $\sigma_i^\pm \equiv S_i^\pm$. Thus Hamiltonian (S14) is equivalent to the Hamiltonian (1) from the Main text up to the replacement of square lattice by the Cayley tree. Full coordination number of sites of CT is $Z = K + 1$ and we have in mind correspondence to original square lattice, so the "most realistic" value of branching number is $K = 3$.

Our main goal is to derive, using loopless structure of the Cayley tree, a kind of recursion relations between i) local relaxation rates Γ_i^r for spins which belong to different sites i of the CT, and ii) local dephasing rates Γ_i^ϕ for the same spins. To realize this program, it will be useful to represent Heisenberg equations for spin operators in the form similar to Schrodinger equations for wavefunctions. The advantage of this approach is that it keeps track of local nature of interactions in the Hamiltonian (S14), which is somewhat hidden in many-body wavefunctions.

The evolution equation for the operators is a linear equation and to rewrite it as a Schrödinger-type equation we introduce the mixed state of our system with its copy:

$$|\hat{1}\rangle := \bigotimes_j \left[\frac{|00\rangle_j + |11\rangle_j}{\sqrt{2}} \right] = \frac{1}{\sqrt{2^n}} \sum_s |s\rangle \otimes |s\rangle \quad (\text{S15})$$

where n is the total number of spins. In the last terms sum runs over all bit-strings. Using this mixed state we can consider each operator as a wave function in the extended Hilbert space (of original system and its copy):

$$|\hat{O}\rangle = \hat{O} \otimes |\hat{1}\rangle \quad (\text{S16})$$

We note the following useful property: $\hat{O} \otimes |\hat{1}\rangle = |\hat{1}\rangle \otimes \hat{O}^T |\hat{1}\rangle$. The evolution equation acquires then the following form:

$$\begin{aligned} i\partial_t |\hat{O}(t)\rangle &= \mathcal{H} |\hat{O}(t)\rangle \equiv |[\hat{O}(t), H]\rangle \quad \text{where} \\ \mathcal{H} &= \hat{1} \otimes H^T - H \otimes \hat{1} \end{aligned} \quad (\text{S17})$$

Below we consider Hamiltonian (S14) as a sum $H = H_0 + V$ where "bare Hamiltonian" H_0 coincides with the second sum in (S14) while "perturbation" V is given by the first term. The states $|\sigma_j^z\rangle, \sqrt{2}|\sigma_j^\pm\rangle$ (in the extended Hilbert space) are normalized eigenstates of \mathcal{H}_0 with eigenvalues 0 and $\pm h_j$ respectively.

The action of the perturbation \mathcal{V} on the operators σ_j^z and σ_j^\pm is as follows:

$$\begin{aligned} \mathcal{V}|\sigma_j^z\rangle &= J \sum_{k \in \partial j} [|\sigma^z, \sigma_j^+ \sigma_k^- + \sigma_j^- \sigma_k^+\rangle] \\ &= 2J \sum_{k \in \partial j} (|\sigma_j^+ \sigma_k^- \rangle - |\sigma_j^- \sigma_k^+ \rangle) \end{aligned} \quad (\text{S18})$$

and

$$\mathcal{V}|\sigma_j^\pm\rangle = \pm J \sum_{k \in \partial j} |\sigma_j^z \sigma_k^\pm\rangle \quad (\text{S19})$$

Here $k \in \partial j$ means that k is a neighbor of j .

Now we calculate relaxation rate Γ^\pm in this spin model. The relaxation rate is given by the imaginary part of the self-energy Σ_z which reads:

$$\Sigma_z(\epsilon) = \text{Im} \langle \sigma_j^z | \mathcal{V} (\epsilon - \mathcal{H} + i0)^{-1} \mathcal{V} | \sigma_j^z \rangle \quad (\text{S20})$$

Now we use approximation of high connectivity, $K \gg 1$. It allows us to consider dynamics of neighboring spins being weakly correlated, thus $\langle \sigma_j^+(t) \sigma_k^+(t) | \sigma_j^+ \sigma_k^+ \rangle \approx \langle \sigma_j^+(t) | \sigma_j^+ \rangle \langle \sigma_k^+(t) | \sigma_k^+ \rangle$. This is a kind of self-consistent born approximation, like the one used in Ref. [1]. The resulting self-energy for z -component of spin is given by:

$$\begin{aligned} \Sigma_z^{(j)}(\epsilon) = 2J^2 \sum_{k \in \partial} & [\langle \sigma_k^- | (\epsilon - h_j - \mathcal{H} + i0)^{-1} | \sigma_k^- \rangle + \\ & \langle \sigma_k^+ | (\epsilon + h_j - \mathcal{H} + i0)^{-1} | \sigma_k^+ \rangle] \end{aligned} \quad (\text{S21})$$

In the same way, self-energy for σ^\pm components can be found in the form

$$\Sigma_\pm^{(j)}(\epsilon) = 2J^2 \sum_{k \in \partial j} \langle \sigma_k^\pm | (\epsilon - \mathcal{H} + i0)^{-1} | \sigma_k^\pm \rangle \quad (\text{S22})$$

4.B. Recursion equations for the relaxation rates

Relaxation rate Γ_j can be found either via the imaginary part of $\Sigma_z^{(j)}(\epsilon)$ at very low energy $\epsilon \rightarrow 0$ or via the imaginary part of $\Sigma_\pm^{(j)}(\epsilon)$ at $\epsilon = h_j$. Calculations of $\text{Im} \Sigma$ using Eq.(S21) in the first case, or Eq.(S22) in the second case, lead to identical results, so we obtain the following self-consistent equation for Γ_j^\pm :

$$\Gamma_j^\pm = J^2 \sum_{k \in \partial j} \frac{\Gamma_k^\pm}{(h_j - h_k)^2 + (\Gamma_k^\pm)^2} \quad (\text{S23})$$

Summation in Eq.(S23) goes over K descendants of the site j . Below in Sec. 5 we will find critical magnitude of $J_r = j_r W$ such that at $J > J_r$ recursions (S23) lead to nonzero relaxation rates Γ_j^\pm .

4.C. Calculation of dephasing rates

a. Schrieffer - Wolff transformation

Now suppose we consider range of couplings $J < J_r$ where lowest-order perturbation theory over J/W does not lead to relaxation and dephasing; in other terms, recursion relations (S23) leads to trivial solution with vanishing Γ^\pm . We are going to show that in fact this result does not mean that dephasing is really absent in our system. To demonstrate it, we study second-order processes, which may lead to *pure dephasing* without relaxation.

It is convenient to employ Schrieffer - Wolff unitary transformation generated by anti-hermitian operator U .

Then the effective Hamiltonian becomes of the form

$$H_{eff} = H + [H, U] + \frac{1}{2} [[H, U], U] + \dots \quad (\text{S24})$$

We are going to find operator U such that H_{eff} will not contain terms which are linear in J and proportional σ_j^\pm . Let $U = \sum_{\langle j, k \rangle} s_{jk} (\sigma_j^+ \sigma_k^- - \sigma_j^- \sigma_k^+)$. Then we need to obey

$$[H_0, U] + V = 0. \quad (\text{S25})$$

The above equation gives: $s_{jk} = J/(h_j - h_k)$. Then the effective Hamiltonian is $H_{eff} = H_0 + V_{eff}$ where $V_{eff} = \frac{1}{2}[V, U]$. Calculating the commutator, we find

$$V_{eff} = \frac{J}{2} \sum_{\langle j,k \rangle} \sum_{\langle l,m \rangle} s_{jk} [\sigma_l^+ \sigma_m^- + \sigma_l^+ \sigma_m^-, \sigma_j^+ \sigma_k^- - \sigma_k^+ \sigma_j^-] \quad (\text{S26})$$

The commutator in Eq.(S26) is not vanishing if the edges (j, k) and (l, m) coincide or have at least one common vertex. Thus we can rewrite V_{eff} as follows:

$$V_{eff} = \frac{J}{2} \sum_{\langle j,k \rangle} s_{jk} (\sigma_k^z - \sigma_j^z) - \frac{J}{2} \sum_j \sum_{(l,k) \in \partial j} (s_{jk} + s_{lj}) \sigma_j^z (\sigma_l^+ \sigma_k^- + \sigma_l^- \sigma_k^+) \quad (\text{S27})$$

Here sign $(l, k) \in \partial j$ means that the sum runs over all possible pairs of neighbors of j -th vertex. Effective perturbation Hamiltonian (S27) will be used below to calculate dephasing rates.

b. Recursion equations for dephasing

We will use the formalism of the previous Subsection to find a dephasing rate, with a focus on dynamics of operator σ_j^+ . The action of the perturbation V_{eff} on a σ_j^+ can be written, in the extended space, in the form

$$\mathcal{V}_{eff} |\sigma_j^+\rangle \approx \sum_{(m,k) \in \partial j} (s_{jk} + s_{mj}) |\sigma_j^+ (\sigma_k^+ \sigma_m^- + \sigma_k^- \sigma_m^+)\rangle \quad (\text{S28})$$

Note, that we take into account the terms proportional to σ_j^z only, while other terms which are usually responsible for decay process are neglected; the reason is our assumption that J/W is too small to generate decay self-consistently.

The corresponding self-energy is:

$$\begin{aligned} \Sigma_j^+(\epsilon) &= 4J^2 \sum_{(m,k) \in \partial j} (s_{jk} + s_{jm})^2 \langle \sigma_k^+ \sigma_m^- | (\epsilon - h_j - \mathcal{H}_{eff} + i0)^{-1} | \sigma_k^+ \sigma_m^- \rangle \approx \\ &4J^2 \sum_{(m,k) \in \partial j} (s_{jk}^2 + s_{jm}^2) \langle \sigma_k^+ \sigma_m^- | (\epsilon - h_j - \mathcal{H}_{eff} + i0)^{-1} | \sigma_k^+ \sigma_m^- \rangle \end{aligned} \quad (\text{S29})$$

The dephasing rate Γ^ϕ is given by the imaginary part of the self-energy $\text{Im} \Sigma_j^+(\epsilon)$ at $\epsilon = h_j$. To estimate a correlation function of the operator $\sigma_k^+ \sigma_m^-$ we use large connectivity limit $K \gg 1$ and suppose that this correlation function is factorized in the time domain, due to weak correlations between different spins; the same approximation was used in the previous Section while deriving Eq.(S21,S22). The resulting equation for the self-energy reads as follows:

$$\begin{aligned} \Sigma_j^+(h_j + \delta\epsilon) &= 4J^2 \sum_{(m,k) \in \partial j} (s_{jk}^2 + s_{jm}^2) i \int \frac{d\epsilon_1}{2\pi} \langle \sigma_k^+ | (\epsilon_1 - \mathcal{H}_{eff} + i0)^{-1} | \sigma_k^+ \rangle \times \\ &\langle \sigma_m^- | (\delta\epsilon - \epsilon_1 - \mathcal{H}_{eff} + i0)^{-1} | \sigma_m^- \rangle \approx J^2 \sum_{(m,k) \in \partial j} \frac{s_{jk}^2 + s_{jm}^2}{h_m - h_k + i(\Gamma_k^\phi + \Gamma_m^\phi)} \end{aligned} \quad (\text{S30})$$

Calculating the imaginary part of the above self-energy we find the (linearized form of) recursion equation for the dephasing rate:

$$\Gamma_j^\phi = J^4 \sum_{(m,k) \in \partial j} \left(\frac{1}{(h_j - h_k)^2} + \frac{1}{(h_j - h_m)^2} \right) \frac{\Gamma_k^\phi + \Gamma_m^\phi}{(h_k - h_m)^2} \quad (\text{S31})$$

Recursion equation (S31) will be used below in Sec.5 for determination of the threshold value $j_c = J_c/W$ for the existence of self-consistent dephasing in our spin system.

5. THRESHOLDS FOR THE RELAXATION AND DEPHASING CHANNELS

5.A. “Upper limit” approximation

a. Relaxation rate

At very small J/W we can neglect correlations between Γ_i^r at some site i and local field h_i ; it amounts to setting $h_0 = 0$ in Eq.(S23). Then these equations become identical to those derived in Ref. [78] for Anderson localization on a tree (of branching number K), within simplest “upper limit” approximation that neglects level repulsion (in other terms, real part of self-energy is neglected). The critical value $j_r = J_r/W$ can be found from the analysis of the linearized version of Eq.(S23). Instability point of this linear recursion (with Γ^\pm neglected in denominator in R.H.S.) is determined by the set of two equations

$$\frac{dF}{dx} \Big|_{x=x_*} = 0; \quad F(x_*) = 0 \quad (\text{S32})$$

where $F(x) \rightarrow F_1(x)$ and

$$F_1(x) = \frac{1}{x} \ln \left\{ K \int P_0(h) dh [J^2 \cdot f(h)]^x \right\}; \quad f(h) = 1/h^2 \quad (\text{S33})$$

where $P_0(h) = (1/W)\theta(\frac{W}{2} - |h|)$. Equations (S32,S33) can be derived using theory of freezing transition for random polymers on a tree [80, 81]. Solving the above set of equations one finds algebraic equation

$$\frac{1}{2j_r} = eK \ln \frac{1}{2j_r} \quad (\text{S34})$$

Its solution for $K = 3$ is $j_r \approx 1.86 \cdot 10^{-2}$.

b. Dephasing rate

Generalizing the procedure described in the above Subsection for recursion equations (S31), one can find critical value $j_\phi = J_\phi/W$ by means of the same Eqs.(S32) but with $F(x)$ function replaced by another function $F_2(x)$ where

$$F_2(x) = \frac{1}{x} \ln \left\{ K^2 \iint_{-1/2}^{1/2} dh_1 dh_2 [J^4 \cdot f(h_1, h_2)]^x \right\} \quad (\text{S35})$$

where

$$f(h_1, h_2) = \frac{1}{(h_1 - h_2)^2} \left(\frac{1}{h_1} + \frac{1}{h_2} \right)^2 \quad (\text{S36})$$

Equations (S35,S36) can be derived along the line of ideas present in Refs. [80, 81]. We introduce Laplace transform $G(e^{-x})$ of the probability density function $\mathcal{P}(\Gamma_j)$ where evolution of Γ_j along the recursion follows Eq.(S31). Then, instead of Eq.(9) of Ref. [81] we come to

$$G_{L+1}(x) = \prod_{\mu=1}^{K(K-1)/2} \int \rho(\epsilon_\mu) d\epsilon_\mu G_L^2(x + \epsilon_\mu) \quad (\text{S37})$$

where μ stays for a pair of indices j, m staying in the R.H.S. of Eq.(S31), number of such pairs is $K(K-1)/2$. Density of the distribution $\rho(\epsilon)d\epsilon$ is determined by the original distribution of local fields $P_0(h_1, h_2) = W^{-2}\theta(\frac{W}{2} - |h_1|)\theta(\frac{W}{2} - |h_2|)$ and by the function (S36) that corresponds to the h -dependent factor in Eq.(S31) after we set $h_j \rightarrow 0$, as it was done in the beginning of Sec. II A 1 above. Second power of the characteristic function G comes about in Eq.(S37) due to the presence of two random variables Γ_k, Γ_m in the R.H.S. of Eq.(S31). General properties of the characteristic function $G(x)$ are the same as in the original approach [80, 81]. In particular, freezing transition point is determined by its far right asymptotics $x \rightarrow \infty$ where $1 - G(x) \equiv g(x) \ll 1$, and thus $G^2(x) \approx 1 - 2g(x)$. Due to that fact, we

come to Eq.(S35), where we also replaced $K(K-1) \rightarrow K^2$ in the large- K limit.

Approximate integration in Eq.(S35) and use of (S32) gives

$$\frac{1}{j_c(2\sqrt{2}+2)^{1/2}} = eK \ln \frac{\sqrt{\alpha_1}}{j_c} \quad (\text{S38})$$

where $\alpha_1 \sim 1$. It follows from Eqs.(S38,S34) that $j_\phi < j_r$ in general. For $K = 3$ numerical integration in Eq.(S35) leads to $j_\phi = 1.4 \cdot 10^{-2}$. In a similar way, we find critical values j_r and j_c for several other branching numbers K , the results are summarized in the Table 1.

K	3	4	5	6
j_r	$1.86 \cdot 10^{-2}$	$1.24 \cdot 10^{-2}$	$0.92 \cdot 10^{-2}$	$0.72 \cdot 10^{-2}$
j_c	$1.4 \cdot 10^{-2}$	$1.0 \cdot 10^{-2}$	$0.8 \cdot 10^{-2}$	$0.6 \cdot 10^{-2}$

5.B. Account for self-energy correction

a. Relaxation rate threshold

Much better analytical approximation was proposed for the problem that is very similar to the one defined by Eq.(S23), in Ref. [79]. They show that self-energy effects may be accounted for by the replacement of bare distribution $P_0(h)$ by *effective* distribution function $P_1(h)$

$$P_1(h) = \frac{1}{W - 4J^2/W} \theta\left(\frac{W}{2} - |h|\right) \theta\left(|h| - \frac{2J^2}{W}\right) \quad (\text{S39})$$

which accounts for the absence of too small resonance denominators in the R.H.S. of Eq.(S23), due to self-energy corrections. An important feature of the distribution (S39) is its symmetry: $P_1(h/W) = P_1(W/h)$. Due to this symmetry, one does not need to optimize over the value of exponent x , as it was done in Sec.2A above. It was shown already in Ref. [78] that the optimal exponent is now $x = 1/2$. Instead of two equations in Eq.(S32), we put $x = 1/2$ into the definition of function $F(x)$ in Eq.(S33) and use the second equation of Eqs.(S32) only: $F_1(\frac{1}{2}) = 0$. Then the critical value $j_r = J_r/W$ can be found [79] from

$$KJ \int P_1(h) \frac{dh}{h} = 1 \quad (\text{S40})$$

Using Eq.(S39) we get then an algebraic equation

$$\frac{1}{2j_r} - 2j_r = 2K \ln \frac{1}{2j_r} \quad (\text{S41})$$

whose solution is $j_r \approx 0.03$ for $K = 3$ in very good agreement with numerical results [82] (agreement persists for other values of K as well).

b. Dephasing rate threshold

Main idea for account of $\text{Re} \Sigma$ is the same as in the above Subsection: we use $x = 1/2$ and integrate over region on the plane (h_1, h_2) where $|\text{Re} \Sigma| < W/2$ and also both $|h_{1,2}| < W/2$. Specifically, we need to solve

$$J^2 K^2 \int dh_1 dh_2 P_2(h_1, h_2) \left| \frac{1}{h_1} + \frac{1}{h_2} \right| \frac{1}{|h_1 - h_2|} = 1 \quad (\text{S42})$$

with renormalized distribution

$$P_2(h_1, h_2) = \frac{1+a}{W^2} \theta\left(\frac{W}{2} - |S|\right) \theta\left(\frac{W}{2} - |h_1|\right) \theta\left(\frac{W}{2} - |h_2|\right)$$

where

$$S \equiv \text{Re} \Sigma = J^4 \left(\frac{1}{h_1} + \frac{1}{h_2} \right)^2 \frac{1}{|h_1 - h_2|} \quad (\text{S43})$$

and $a \ll 1$ accounts for the change of normalization of the distribution due to restriction $|s| < W/2$; this is very small effect which can be neglected.

In dimensionless units (setting $W = 1$ and changing $J \rightarrow j$), we need to solve for the value of j the following equation (main interest is in $K = 3$):

$$\int_{-1/2}^{1/2} \int_{-1/2}^{1/2} dx dy \left| \frac{1}{x} + \frac{1}{y} \right| \frac{\theta(\frac{1}{2} - |s|)}{|x - y|} = \frac{1}{j^2 K^2} \quad (\text{S44})$$

where

$$s = j^4 \left(\frac{1}{x} + \frac{1}{y} \right)^2 \frac{1}{|x - y|}$$

Numerical solution for $K = 3$ leads to $j_c = 0.02$. Ratio $j_r/j_c = 1.5$. In a similar way, we find critical values j_r and j_c for several other branching numbers K , the results are summarized in the Table 2.

K	3	4	5	6
j_r	$3.0 \cdot 10^{-2}$	$1.95 \cdot 10^{-2}$	$1.4 \cdot 10^{-2}$	$1.1 \cdot 10^{-2}$
j_c	$2.0 \cdot 10^{-2}$	$1.3 \cdot 10^{-2}$	$1.0 \cdot 10^{-2}$	$0.75 \cdot 10^{-2}$

Results collected in Table 1 and Table 2 demonstrate that $j_c < j_r$ for all various values of K and within two different approximation schemes.